



Originally published as:

Bosch, C., Andersson, A., Kirillova, E. N., Budhavant, K., Tiwari, S., Praveen, P., Russell, L. M., Beres, N. D., Ramanathan, V., Gustafsson, Ö. (2014): Source-diagnostic dual-isotope composition and optical properties of water-soluble organic carbon and elemental carbon in the South Asian outflow intercepted over the Indian Ocean. - *Journal of Geophysical Research: Atmospheres*, 119, p. 11,743-11,759.

DOI: <http://doi.org/10.1002/2014JD022127>

## RESEARCH ARTICLE

10.1002/2014JD022127

## Key Points:

- Fossil fuel contribution to PM<sub>2.5</sub> EC and WSOC is 41% and 14% respectively
- Aerosol LRT leads to <sup>13</sup>C enrichment and a less absorbing WSOC aerosol
- WSOC accounts for only ~ 1% of direct solar absorbance relative to EC

## Supporting Information:

- Readme
- Figure S1
- Figure S2
- Figure S3
- Figure S4
- Figure S5
- Figure S6
- Table S1
- Table S2
- Table S3
- Table S4
- Table S5
- Table S6
- Table S7

## Correspondence to:

Ö. Gustafsson,  
orjan.gustafsson@itm.su.se

## Citation:

Bosch, C., A. Andersson, E. N. Kirillova, K. Budhavant, S. Tiwari, P. S. Praveen, L. M. Russell, N. D. Beres, V. Ramanathan, and Ö. Gustafsson (2014), Source-diagnostic dual-isotope composition and optical properties of water-soluble organic carbon and elemental carbon in the South Asian outflow intercepted over the Indian Ocean, *J. Geophys. Res. Atmos.*, 119, 11,743–11,759, doi:10.1002/2014JD022127.

Received 5 JUN 2014

Accepted 10 SEP 2014

Accepted article online 12 SEP 2014

Published online 18 OCT 2014

## Source-diagnostic dual-isotope composition and optical properties of water-soluble organic carbon and elemental carbon in the South Asian outflow intercepted over the Indian Ocean

Carme Bosch<sup>1</sup>, August Andersson<sup>1</sup>, Elena N. Kirillova<sup>1</sup>, Krishnakant Budhavant<sup>2</sup>, Suresh Tiwari<sup>3</sup>, P. S. Praveen<sup>2,4</sup>, Lynn M. Russell<sup>5</sup>, Nicholas D. Beres<sup>6</sup>, Veerabhadran Ramanathan<sup>5</sup>, and Örjan Gustafsson<sup>1</sup>

<sup>1</sup>Department of Applied Environmental Science and Bolin Centre for Climate Research, Stockholm University, Stockholm, Sweden, <sup>2</sup>Maldives Climate Observatory at Hanimaadhoo, Hanimaadhoo, Republic of the Maldives, <sup>3</sup>Indian Institute of Tropical Meteorology (Branch), New Delhi, India, <sup>4</sup>Institute for Advanced Sustainability Studies, Potsdam, Germany, <sup>5</sup>Scripps Institution of Oceanography, University of California, San Diego, La Jolla, California, USA, <sup>6</sup>Division of Atmospheric Sciences, Desert Research Institute, Nevada System of Higher Education, Reno, Nevada, USA

**Abstract** The dual carbon isotope signatures and optical properties of carbonaceous aerosols have been investigated simultaneously for the first time in the South Asian outflow during an intensive campaign at the Maldives Climate Observatory on Hanimaadhoo (MCOH) (February and March 2012). As one component of the Cloud Aerosol Radiative Forcing Dynamics Experiment, this paper reports on the sources and the atmospheric processing of elemental carbon (EC) and water-soluble organic carbon (WSOC) as examined by a dual carbon isotope approach. The radiocarbon ( $\Delta^{14}\text{C}$ ) data show that WSOC has a significantly higher biomass/biogenic contribution ( $86 \pm 5\%$ ) compared to EC ( $59 \pm 4\%$ ). The more <sup>13</sup>C-enriched signature of MCOH-WSOC ( $-20.8 \pm 0.7\text{‰}$ ) compared to MCOH-EC ( $-25.8 \pm 0.3\text{‰}$ ) and megacity Delhi WSOC ( $-24.1 \pm 0.9\text{‰}$ ) suggests that WSOC is significantly more affected by aging during long-range transport than EC. The  $\delta^{13}\text{C}-\Delta^{14}\text{C}$  signal suggests that the wintertime WSOC intercepted over the Indian Ocean largely represents aged primary biomass burning aerosols. Since light-absorbing organic carbon aerosols (Brown Carbon (BrC)) have recently been identified as potential contributors to positive radiative forcing, optical properties of WSOC were also investigated. The mass absorption cross section of WSOC ( $\text{MAC}_{365}$ ) was  $0.5 \pm 0.2 \text{ m}^2 \text{ g}^{-1}$  which is lower than what has been observed at near-source sites, indicating a net decrease of WSOC light-absorption character during long-range transport. Near-surface WSOC at MCOH accounted for ~1% of the total direct solar absorbance relative to EC, which is lower than the BrC absorption inferred from solar spectral observations of ambient aerosols, suggesting that a significant portion of BrC might be included in the water-insoluble portion of organic aerosols.

### 1. Introduction

High loadings of carbonaceous aerosols in South Asia are of large concern for causing severe adverse effects on human health and regional climate [e.g., Brunekreef and Forsberg, 2005; Lawrence and Lelieveld, 2010; Ramanathan et al., 2001]. Anthropogenic emissions from fossil fuel and biomass combustion are generally high throughout the Indian subcontinent and adjacent areas and particularly exacerbated over the Indo-Gangetic Plain, one of the most populated regions in the world [Ramanathan and Carmichael, 2008; Zhang et al., 2009] (Figure 1).

Carbonaceous aerosols (CA) are composed of organic carbon (OC) and black carbon (BC, or elemental carbon (EC)). BC, a primary pollutant formed during the incomplete combustion of carbonaceous matter, consists of aggregates of small carbon spherules and is insoluble in water and in other organic solvents. In contrast, OC is a mixture of primary and secondary organic aerosols since this fraction undergoes physical and chemical formation and transformations in the atmosphere. Knowledge about CA sources, which may be of both anthropogenic and biogenic origins, is a prerequisite for both improved system understanding and for guiding effective policy measures aimed at mitigating anthropogenic aerosol emissions. Radiocarbon analysis has been reported to be a powerful technique for source apportionment for

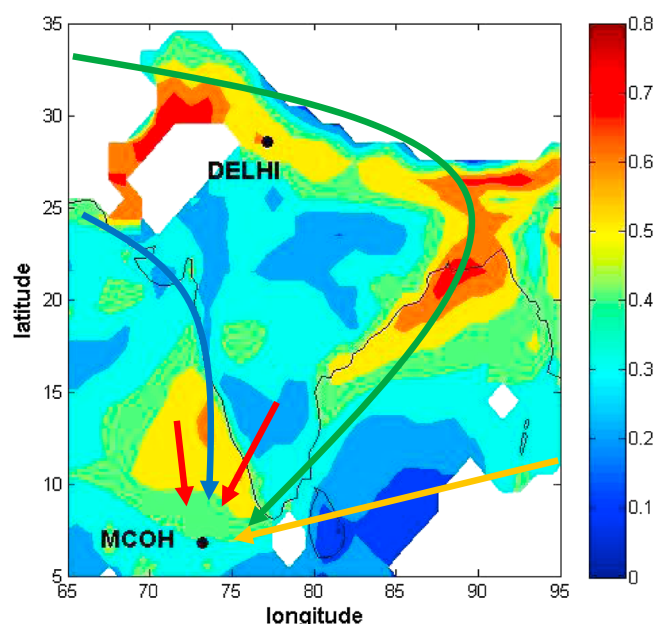


**Figure 1.** Map depicting average Aerosol Optical Depth (AOD) during the CARDEX campaign (23 February to 31 March 2012). The locations of the Maldives Climate Observatory at Hanimaadhoo (MCOH) and Delhi are shown. Colored arrows show the predominant BTs differentiated in four different clusters: IGP and Bay of Bengal (dark green), South India (red), Arabian Sea (blue), and southern Bay of Bengal (dark yellow). AOD data was obtained from NASA Moderate Resolution Imaging Spectroradiometer (MODIS) Level 1 (<http://ladsweb.nascom.nasa.gov/index.html>).

both BC aerosols [Chen *et al.*, 2013; Gustafsson *et al.*, 2009; Liu *et al.*, 2013a; Sheesley *et al.*, 2012; Szidat *et al.*, 2004; Zhang *et al.*, 2014] and the OC components [Kirillova *et al.*, 2013, 2014a, 2014b; Weber *et al.*, 2007; Wozniak *et al.*, 2012].

Black carbon (BC) is a strong absorber of solar radiation. The globally averaged climate forcing due to BC aerosols has recently been bounded to  $+1.1 \text{ W m}^{-2}$  with uncertainty ranging from  $+0.17$  to  $+2.1 \text{ W m}^{-2}$  [Bond *et al.*, 2013]. This effect is much higher over South Asia. In contrast to BC, the organic carbon (OC) aerosol has been traditionally considered as purely light-scattering particles but studies have shown OC to also absorb light, predominantly at shorter wavelengths [Alexander *et al.*, 2008; Andreae and Gelencser, 2006; Chakrabarty *et al.*, 2014; Kirchstetter and Novakov, 2004; Moosmüller *et al.*, 2011; Sun *et al.*, 2007]. These light-absorbing organic aerosols, termed brown carbon (BrC), may thus, next to BC, also contribute to a

positive direct radiative effect on climate ( $+0.04$  to  $+0.11 \text{ W m}^{-2}$  [e.g., Bahadur *et al.*, 2012; Chung *et al.*, 2012; Feng *et al.*, 2013]).

A fraction of BrC has been shown to be water soluble [e.g., Hecobian *et al.*, 2010; Hoffer *et al.*, 2006; Kirillova *et al.*, 2014a; Kirillova *et al.*, 2014b]. Therefore, its dissolution into clouds could result in absorbing droplets that affect the cloud absorption and thus contributing to the semidirect aerosol climate effects [e.g., Jacobson, 2012]. Most climate models do not yet account for BrC absorption. Hence, it is essential to study the source apportionment, the atmospheric processing and optical properties of the water-soluble brown carbon (WS-BrC) component of carbonaceous aerosols.

Water-soluble organic carbon (WSOC) is a large component of carbonaceous aerosols over South Asia with reports ranging from 10 to 65% of the total organic carbon (TOC) [Kirillova *et al.*, 2013, 2014a; Ram *et al.*, 2012; Rengarajan *et al.*, 2011; Srinivas and Sarin, 2014]. However, the primary and secondary sources of WSOC in atmospheric aerosols are still poorly constrained. Biomass burning emissions may be an important primary source of WSOC in the atmosphere [Hoffer *et al.*, 2006; Kirchstetter and Thatcher, 2012; Mohr *et al.*, 2013] while secondary organic aerosol formation from both biogenic and anthropogenic precursors may also produce highly water-soluble and light-absorbing compounds [Ding *et al.*, 2013; Kirillova *et al.*, 2014b; Jacobson *et al.*, 1999; Lambe *et al.*, 2013; Saleh *et al.*, 2013; Weber *et al.*, 2007].

The present study is part of the Cloud Aerosol Radiative Forcing Dynamics Experiment (CARDEX), which was conducted during February and March 2012 using as central node the Maldives Climate Observatory at Hanimaadhoo (MCOH), a receptor for the long-distance transport of the South Asian outflow. The unifying objective of CARDEX was to improve the understanding of the semidirect aerosol climate effect. Here we report on radiocarbon ( $\Delta^{14}\text{C}$ ) and stable ( $\delta^{13}\text{C}$ ) carbon isotopic measurements with the objective of shedding light on the origin of both water-soluble organic carbon (WSOC) and elemental carbon (EC, as the mass-based proxy of BC) components in fine (particulate matter ( $\text{PM}_{2.5}$ )) and coarse (total suspended particle (TSP)) aerosols over background South Asia. The light-absorbing properties of WSOC were also compared with identical measurements in megacity New Delhi in the northern India source region to

investigate the dynamics of the absorptive efficiency of WS-BrC component during long-range transport and aging of the South Asian outflow.

## 2. Methods

### 2.1. Aerosol Sampling

The intensive CARDEX campaign was conducted at Maldives Climate Observatory at Hanimaadhoo, Republic of the Maldives (MCOH, 6 m above sea level 6.78°N, 73.18°E) during 23 February to 31 March 2012. The MCOH is a long-term receptor station for the South Asian outflow, since inception in 2004 forming part of the International Atmospheric Brown Cloud project ([www.rrcap.unep.org/abc/](http://www.rrcap.unep.org/abc/)). MCOH is frequently used for intensive campaigns. Detailed information about this observatory can be found in *Ramanathan et al.* [2007]. Aerosols for the isotopic investigations were collected on precombusted quartz fiber filters using high-volume samplers for PM<sub>2.5</sub> (model DH77, Digital A.G. Switzerland) and a custom built suspended particle (TSP) instrument [e.g., *Gustafsson et al.*, 2009]. Sampling collection time was 12 h for PM<sub>2.5</sub> and 7–14 days for TSP samples. Three filter blanks were collected for each sampler throughout the duration of the campaign. The additional records during CARDEX that were used for this <sup>13</sup>C/<sup>14</sup>C-focused study were meteorological data, aerosol physical parameters including a seven wavelength aethalometer (Magee AE-31) for black carbon absorption/extinction and a condensation particle counter (CPC Model 3022, TSI GmbH, Aachen, Germany) for total particle number.

### 2.2. Concentration Measurements of Carbonaceous Aerosols

The aerosol total carbon (TC) and elemental carbon (EC) concentrations were measured with a thermal-optical transmission (TOT) analyzer (Sunset Laboratory, Tigard, OR, USA) using the National Institute for Occupational Safety and Health (NIOSH) 5040 method [*Birch and Cary*, 1996]. The analytical method for concentration measurement of WSOC was described previously [*Kirillova et al.*, 2010, 2014b]. Briefly, WSOC was extracted by ultrasonication and quantified by a high-temperature catalytic oxidation instrument (Shimadzu-TOC-VCPH, Japan). The presently employed water-to-sample ratio was in the range of 0.10–0.24 cm<sup>3</sup> m<sup>-3</sup> (= volume extraction solvent/volume air sampled), which lies well within the optimal water-to-sample range (>0.1 cm<sup>3</sup> m<sup>-3</sup>) suggested by *Psichoudaki and Pandis* [2013]. TC and WSOC concentration values were blank corrected by subtracting an average of the field blanks. The average relative standard deviation of triplicate analysis was 5%, 4%, and 6% for EC, TC, and WSOC respectively. Blank concentrations were used to calculate detection limits as mean ± standard deviation. Detection limit for TC was 0.14 μg m<sup>-3</sup>. No EC was detected in blanks.

### 2.3. Carbon Isotopic Analysis

#### 2.3.1. EC and TOC Isolation

The EC fraction was isolated for off-line <sup>13</sup>C/<sup>12</sup>C and <sup>14</sup>C/<sup>12</sup>C analyses using a method described earlier [e.g., *Chen et al.*, 2013; *Zencak et al.*, 2007a]. Briefly, it employs a standard carbon aerosol TOT analyzer slightly modified to enable cryogenic online user-defined isolation of CO<sub>2</sub> produced from instrument-defined carbon aerosol fractions (e.g., EC) during the NIOSH 5040 (or other) commonly applied and operational EC methods. First, a filter area corresponding to 60–120 μg of EC and TOC for each sample was acidified by fumigation in open glass Petri dishes held in a desiccator over 12 M hydrochloric acid for 24 h to remove carbonates and subsequently dried at 60°C for 1 h. Filter subsamples of 1.5 cm<sup>2</sup> were placed inside the TOT analyzer for oxidation to CO<sub>2</sub>. The CO<sub>2</sub> produced was diverted and purified online through magnesium perchlorate and silver wool traps to remove water and halogen-containing gases, respectively. Subsequently, it was cryotrapped in liquid N<sub>2</sub> and flame sealed in glass ampoules.

#### 2.3.2. WSOC Isolation

The analytical method for isolation of WSOC in order to determine <sup>13</sup>C and <sup>14</sup>C signatures has been described previously [*Kirillova et al.*, 2010]. However, an alternative acidification was employed in the present study. This new method replaces the old acid fumigation of the filter samples by a milder in situ acidification of the freeze-dried water extracts. The new acidification method was previously tested by *Kirillova et al.* [2014b]. Briefly, a filter area corresponding to at least 120 μg of WSOC was extracted in 10 ml of Milli-Q water. The extracts were freeze-dried and then successively redissolved in 150 μL of 1 M hydrochloric acid, in order to decarbonate the samples. The samples were then transferred into precombusted silver capsules and finally evaporated in the oven at 60°C; the dried WSOC samples were then ready for isotope analyses.

### 2.3.3. Stable and Radiocarbon Measurement

The isotope measurements of WSOC isolates and TOC and EC-derived CO<sub>2</sub> were performed at the U.S. National Ocean Sciences Accelerator Mass Spectrometry facility (Woods Hole, MA, USA) as described previously [e.g., Kirillova et al., 2010; McNichol et al., 1992; Pearson et al., 1998; Zencak et al., 2007b].

### 2.4. Calculation of Radiocarbon-Based Source Contributions

Fractional contributions of radiocarbon-extinct fossil fuel sources ( $f_{\text{fossil}}$ ) versus contemporary biomass/biogenic sources can be determined using the isotopic mass balance equation:

$$\Delta^{14}\text{C}_{\text{sample}} = \Delta^{14}\text{C}_{\text{fossil}} \cdot f_{\text{fossil}} + \Delta^{14}\text{C}_{\text{biomass}} \cdot (1 - f_{\text{fossil}}) \quad (1)$$

where  $\Delta^{14}\text{C}_{\text{sample}}$  is the measured radiocarbon content of a sample and  $\Delta^{14}\text{C}_{\text{fossil}}$  is  $-1000\text{‰}$ . The  $\Delta^{14}\text{C}_{\text{biomass}}$  end-member is between  $+50\text{‰}$  and  $+225\text{‰}$ . The first value corresponds to the  $\Delta^{14}\text{C}$  of contemporary CO<sub>2</sub> [Graven et al., 2012], and thus freshly produced biomass. The second value is for the  $\Delta^{14}\text{C}$  of wood logged in the 1990s–2000s [Klinedinst and Currie, 1999; Zencak et al., 2007a]. For Indian biomass burning an end-member value of  $+195\text{‰}$  has been estimated based on the relative contribution from contemporary (meaning 1 year plants) biofuel (17%) and wood fuel (83%) [Gustafsson et al., 2009].  $\Delta^{14}\text{C}_{\text{biomass}}$  of  $+195\text{‰}$  was applied for source contributions of EC and TOC. The biogenic/biomass  $\Delta^{14}\text{C}$  end-member for WSOC, following Kirillova et al. [2013], was set to  $+123\text{‰}$ , which is the mean value of  $+50\text{‰}$  and  $+195\text{‰}$ , assuming equal source contributions to WSOC from biomass burning and biogenic sources.

### 2.5. Absorption Measurements

Light absorption was measured from water extracts. In this way the brown carbon (BrC) can be isolated by dissolution in water avoiding interferences from BC, which is water insoluble. Light-extinction was measured using a Hitachi U2010 ultraviolet-visible absorption spectrophotometer, scanning the wavelength range of 190–1100 nm. The mass absorption cross section at 365 nm ( $\text{MAC}_{365}$ ) was computed according to the Lambert-Beer Law:

$$\text{MAC}_{365} = \frac{(b_{\text{abs}365})}{[\text{WSOC}]} = \frac{(A_{365} - A_{700}) \cdot \ln(10)}{[\text{WSOC}] \cdot l} \quad (2)$$

where  $b_{\text{abs}}$  is the absorption coefficient,  $\text{WSOC}$  is the water-soluble organic carbon concentration in solution,  $l$  is the light-path length (1 cm, for the currently used quartz cuvettes), and  $A$  is the absorbance of the liquid extract (assuming that the scattering contribution to extinction is low) at 365 and 700 nm. Absorbance at 700 nm (average between 695 and 705 nm, where there is no absorption for ambient aerosol water extracts) is used to account for baseline drift during analysis. The relation between absorbance and light transmittance is based on a common logarithm for liquid extracts (equation (3)) but on a natural logarithm for gases. Thus,  $\ln(10)$  converts from common logarithm (base 10) to natural logarithm. Liquid absorption of the liquid extracts ( $A$ ) is defined as

$$A_{\lambda} = -\log_{10}\left(\frac{I}{I_0}\right) \quad (3)$$

where  $I_0$  and  $I$  are the intensities of the incident light and the transmitted light, respectively. To enable comparison with previous results, the MAC is presented at 365 nm [Cheng et al., 2011; Hoffer et al., 2006; Kirillova et al., 2014a, 2014b; Srinivas and Sarin, 2013, 2014; Zhang et al., 2013]. The wavelength ( $\lambda$ ) dependence of the WSOC absorption was investigated by fitting an Absorption Ångström Exponent (AAE) using the following relation:

$$\frac{A_{\lambda_1}}{A_{\lambda_2}} = \left(\frac{\lambda_2}{\lambda_1}\right)^{\text{AAE}} \quad (4)$$

The AAE was fitted within the range 330–400 nm to avoid interference from other light-absorbing solutes such as ammonium nitrate, sodium nitrate, and nitrate ions which absorb light at peaks near 308, 298, and 302 nm, respectively [Cheng et al., 2011; Jacobson, 1999; Kirillova et al., 2014b]. There may also be an effect of pH on differences in absorptivity between molecular and anions but the effect is likely less for the majority of organic molecules [Jacobson, 1999].

## 2.6. Calculation of the Direct Solar Absorbance of WS-BrC Relative to EC

The amount of solar energy absorbed by water-soluble brown carbon (WS-BrC; i.e., light-absorbing WSOC) relative to elemental carbon (EC) at ground level is estimated using a simplistic model. The fraction ( $f$ ) solar energy absorbed by WS-BrC relative to EC is calculated as

$$f = \frac{\int I(\lambda) \cdot \left\{ 1 - e^{-\left( \text{MAC}_{365, \text{WSOC}} \left( \frac{365}{\lambda} \right)^{\text{AAE}_{\text{WSOC}}} \cdot [\text{WSOC}] \cdot h_{\text{ABL}} \right)} \right\} d\lambda}{\int I(\lambda) \cdot \left\{ 1 - e^{-\left( \text{MAC}_{550, \text{EC}} \left( \frac{550}{\lambda} \right) \cdot [\text{EC}] \cdot h_{\text{ABL}} \right)} \right\} d\lambda} \quad (5)$$

where  $I(\lambda)$  is the clear sky Air Mass 1 Global Horizontal (AM1GH) solar irradiance spectrum at the Earth's surface, which includes light-absorptive effects of, e.g., ozone and water [Levinson *et al.*, 2010];  $\text{MAC}_{365, \text{WSOC}}$  is the mass absorption cross section for WSOC at 365 nm;  $\text{MAC}_{550, \text{EC}}$  is the mass absorption cross section for EC at 550 nm;  $\text{AAE}_{\text{WSOC}}$  is the Absorption Ångström Exponent for WSOC; and  $h_{\text{ABL}}$  is the vertical height of the aerosol layer, here estimated as the height of the boundary layer. The MAC for EC is a matter of considerable debate, but for the current simplistic model we use  $\text{MAC}_{550} = 7.5 \pm 1.2 \text{ m}^2 \text{ g}^{-1}$  and the Absorption Ångström Exponent (AAE) for EC is set to 1 [Bond and Bergstrom, 2006], following Kirillova *et al.* [2014a]. The fraction  $f$  was computed in MATLAB version R2012b (The MathWorks, Natick, MA, USA) with numerical integration (integration step 1 nm, integration interval 300–2500 nm) using measured sample specific values for the concentrations of WSOC and EC, and the optical properties of WSOC ( $\text{MAC}_{365, \text{WSOC}}$  and  $\text{AAE}_{\text{WSOC}}$ ). The  $h_{\text{ABL}}$  is set to 1000 m but has little influence on the computed ratio in the range of 100–3000 m.

This simplistic estimate is based on several assumptions: (a) the AAE of WS-BrC measured at 330–400 nm represents the whole spectral range. Wavelengths lower than 330 nm are discarded to avoid other solute interferences and WSOC absorption at wavelengths greater than 500 nm is almost negligible. In addition the AM1GH solar emission spectrum is rapidly decreasing toward zero for wavelengths shorter than 300 nm. (b) The light-absorptive properties of the solvent extracts are representative of the ambient aerosol phase and there are no effects of scattering or size distributions of aerosols. Although different conversion values ranging from 0.7 to 2 have been reported depending on size-resolved WSOC concentrations elsewhere [Liu *et al.*, 2013b; Sun *et al.*, 2007], here a factor of 1 was assumed for our calculations. (c) The literature-retrieved values for  $\text{MAC}_{550}$  and AAE for EC are reasonable. (d) The measurements at ground level represent a near-surface well-mixed vertical aerosol layer with a height defined by  $h_{\text{ABL}}$ . It is stressed that there is no implication of a column-integrated relative radiative effect of WS-BrC versus EC, which are likely to have a nonhomogenous vertical distribution [e.g., Liu *et al.*, 2014; Samset and Myhre, 2011]; the aim of the calculation is to broadly evaluate the solar spectrum integrated relative absorbance of WS-BrC and EC for a ground-level situation over the Indian Ocean. A sensitivity analysis, examining the influence of the required assumptions has been included in the supporting information (Figure S6).

## 2.7. Fourier Transform Infrared Measurements

Organic matter (OM) functional groups were determined by Fourier transform infrared (FTIR) spectroscopy at Scripps Institution of Oceanography (University of California, San Diego, USA). Submicron particles were collected on 37 mm Teflon filters (Pall Inc., 37 mm diameter, 1.0  $\mu\text{m}$  pore size) downstream of a 1  $\mu\text{m}$  sharp cut cyclone (SCC 2.229 PM<sub>1</sub>, BGI Inc.). The aerosol particles were dried (Silica orange gel 13767, Sigma-Aldrich, USA) to below 25% relative humidity prior to the cyclone. Back filters were also collected to quantify VOC adsorption and artifacts; however, absorbance on all back filters was below limit of detection. To reduce evaporative losses, samples were stored and transported at 0°C prior to analysis with a Tensor 27 FTIR spectrometer equipped with a DTGS detector (Bruker, Billerica, MA). Organic functional groups were quantified from FTIR absorbance spectra [Gilardoni *et al.*, 2007] using an automated peak-fitting algorithm described by Takahama *et al.* [2013]. Organic functional groups that were above the limit of quantification in at least 20% of the samples were saturated aliphatic C-CH (alkane), nonacid organic hydroxyl C-OH (alcohol), primary amine C-NH<sub>2</sub>, nonacid carbonyl C=O (aldehyde, ketone, or ester carbonyl), and carboxylic acid COOH groups.

## 2.8. Ion Analysis

Mass concentrations of nitrate (NO<sub>3</sub><sup>-</sup>), sulfate (SO<sub>4</sub><sup>2-</sup>), ammonium (NH<sub>4</sub><sup>+</sup>), sodium (Na<sup>+</sup>), and potassium (K<sup>+</sup>) were determined at the Desert Research Institute (Reno, NV). Water-soluble NO<sub>3</sub><sup>-</sup> and SO<sub>4</sub><sup>2-</sup> concentrations were measured by ion chromatography (IC) (Dionex ICS-3000, Sunnyvale, CA) [Chow and Watson, 1999] where

water extracts from each quartz fiber filter were injected into the IC operating at  $2.0 \text{ mL min}^{-1}$ . The Dionex system contains a guard column and an anion separator column with a strong basic anion exchange resin, and an anion micromembrane suppressor column with a strong acid ion exchange resin. The anion eluent consisted of sodium carbonate ( $\text{Na}_2\text{CO}_3$ ) and sodium bicarbonate ( $\text{NaHCO}_3$ ) prepared in double-distilled water.

Water-soluble ammonium ( $\text{NH}_4^+$ ) was measured by colorimetry using the Astoria Pacific Automated Colorimetric System (Astoria Pacific, Clackamas, OR) [Fung *et al.*, 1979; Sandell, 1959]. A computer-controlled autosampler housed 2 mL of sample extract, where the liquid's absorbance, related to the ion concentration through Beer-Lambert law, was measured at 630 nm through an interference filter specific to the species being measured.

Water-soluble  $\text{Na}^+$  and  $\text{K}^+$  concentrations were measured by atomic absorption spectrophotometry using a SpectrAA-880 Double Beam atomic absorption spectrometer (Varian, Palo Alto, CA) [Butler *et al.*, 2009; Fernandez, 1989; Rhodes *et al.*, 1989]. One to two milliliters of the quartz fiber filter sample extracts were aspirated into an acetylene airflame at  $0.5 \text{ mL min}^{-1}$ . A hollow-cathode lamp emits wavelengths for each analyte (589 nm for  $\text{Na}^+$  and 766.5 nm for  $\text{K}^+$ ). Stock standard solutions were NIST traceable inductively coupled plasma grade at concentrations levels of  $1 \text{ mg mL}^{-1}$ . Cesium chloride was added to samples and standard solutions to eliminate ionization interference.

### 2.9. Uncertainties

The overall precision in the elemental carbon (EC), total carbon (TC), and water-soluble organic carbon (WSOC) concentrations and isotopic signatures was estimated considering the analytical precision of concentration measurements (estimates from triplicate analysis), mass contributions from field blanks (estimates from several blanks), and the precision of the isotope characterization and the isotope signature of the field blanks. To obtain the overall precision, these factors need to be combined using an error propagation scheme. Here this was implemented using a random sampling Monte Carlo strategy [Andersson, 2011]. In this procedure, the uncertainty for each parameter (e.g., field blank concentration) was represented by a normal distribution with zero mean and a standard deviation equal to the measured uncertainty [Kirillova *et al.*, 2013]. Independent random samplings from the distributions representing the data were performed using an in-house written MATLAB script. For each point, 10,000 iterations of the random sampling scheme were conducted, allowing sufficient sampling of the different combinations.

## 3. Results and Discussion

### 3.1. Meteorological Conditions and Air Mass Characterization During CARDEX

The regional meteorology of South Asia is dominated by the Asian monsoon circulation. During the dry season (November–March) the Intertropical Convergence Zone, where air masses from the meteorological Northern and Southern Hemispheres converge, migrates to lower latitudes (between  $5^\circ\text{S}$  and  $15^\circ\text{S}$ ) with the solar heating. Air masses reaching the Maldives Climate Observatory of Hanimaadhoo (MCOH) during the dry season have generally originated over the Indian subcontinent.

Since MCOH is located downwind of the Indian subcontinent during the dry winter season, it affords the possibility to intercept the anthropogenic outflow from mainland South Asia. Seven day back trajectories (BTs) were generated at 500 m for every 12 h using NOAA Hybrid Single-Particle Lagrangian Integrated Trajectory (HYSPLIT) software v4 (<http://www.arl.noaa.gov/ready/hysplit4.html>). Air mass back trajectories for CARDEX showed a clear predominance of air coming from the Indian subcontinent and adjacent land and sea areas. Seven day air mass back trajectories from this campaign were grouped into four different clusters (Figures 1 and S1). The four different origin/source clusters are the following: Indo-Gangetic Plain (IGP) and central Bay of Bengal, southern India, central and eastern Arabian Sea (including western Indian margin), and southern Bay of Bengal. Air masses from the IGP-Bangladesh-Bay of Bengal source continuum are associated with high aerosol loadings (Figures 1 and 2a).  $\text{PM}_{2.5}$  mass concentrations were  $21.4 \pm 11.3 \mu\text{g m}^{-3}$  ( $n = 67$ ) with 23 samples out of 67 found to be above the World Health Organization limit for daily average  $\text{PM}_{2.5}$  samples ( $25 \mu\text{g m}^{-3}$ , [WHO Air Quality Guidelines, 2006]) (Figure S2b).

Back trajectory analyses allowed identifying several different periods during the campaign. A first period, from 23 February to 2 March 2012 (Period I), exhibited a predominant air mass transport from IGP flowing

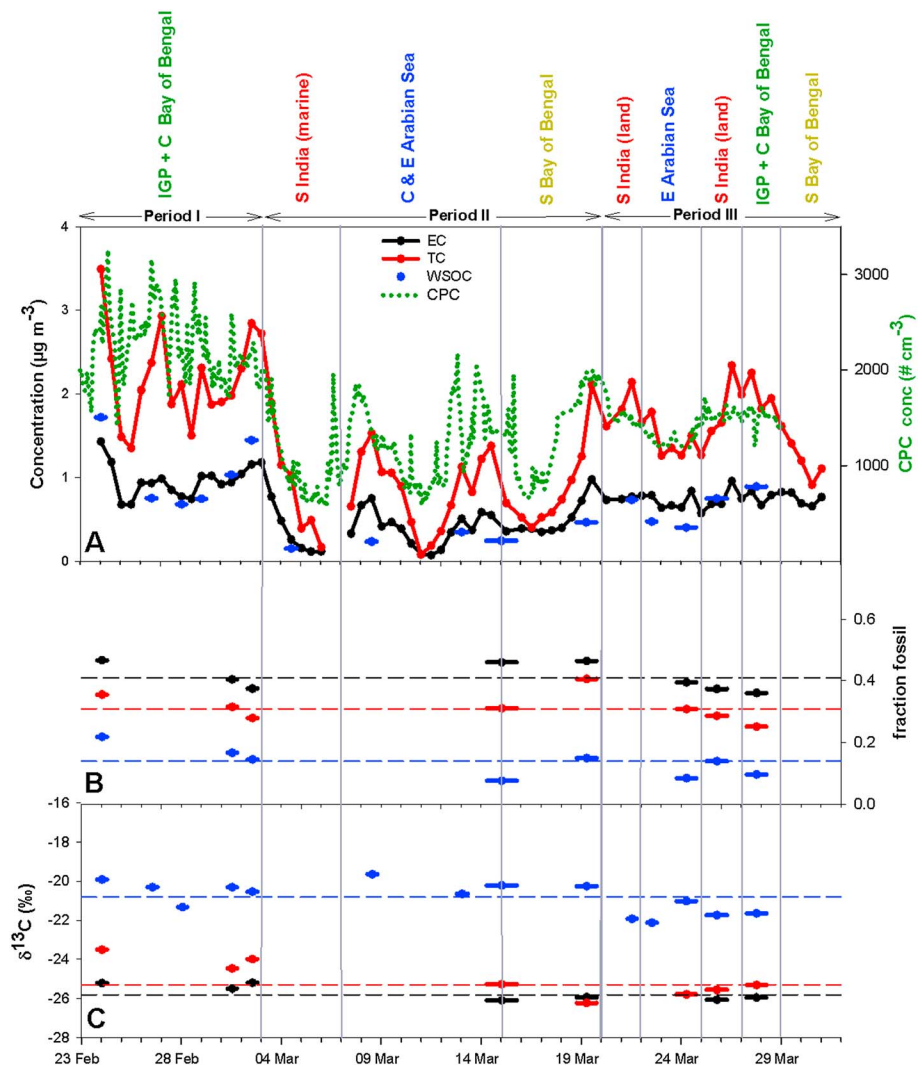


**Figure 2.** Concentrations and isotopic composition of carbonaceous aerosol fractions in the fine ( $PM_{2.5}$ ) size fraction at MCOH; (a) elemental carbon (EC, black), total carbon (TC, red), water-soluble organic carbon (WSOC, blue), and CPC aerosol particle number; (b) radiocarbon-based source apportionment measurements of fraction fossil of elemental carbon (EC, black), total organic carbon (TOC, red), and water-soluble organic carbon (WSOC, blue); and (c) stable carbon isotope ratio of EC, TOC, and WSOC. Back trajectory source clusters are marked at the top. Dashed lines in Figures 2b and 2c indicate observed means of whole period.

southward over the Bay of Bengal before arrival at MCOH (Figures 2 and S1). During this period the highest number of aerosol particles was observed (mean:  $2258 \pm 350 \text{ cm}^{-3}$ ) (Figure 2a). A sudden decrease in aerosol particle concentration was observed on 3 March, likely due to a drift in the air mass origin. From 3 to 19 March (Period II) the number of aerosol particles was distinctly lower (mean:  $1194 \pm 431 \text{ cm}^{-3}$ ). During a first stage in this period air mass originated at the west coast of the southern Indian subcontinent (3 to 6 March), followed by a second period with origins near the Arabian Peninsula and northern Arabian Sea coast with transport along the Indian western coast (7 to 14 March), and a third with air mass coming from south Bay of Bengal (Figure S1). From 20 March onward (Period III) near-surface back trajectories originated mostly in southern and northern India and east Arabian Sea (Figure S1). Number particle concentration during this last period was on average  $1447 \pm 152 \text{ cm}^{-3}$  (Figure 2a).

### 3.2. TOC, EC, and WSOC Concentrations

This is the first time that concentrations of elemental carbon (EC), total carbon (TC = OC + EC), and water-soluble organic carbon (WSOC) are reported simultaneously for the South Asian outflow at MCOH.

Throughout the duration of the campaign, EC and TC concentrations in  $PM_{2.5}$  were  $0.07\text{--}1.4\ \mu\text{g m}^{-3}$  (mean:  $0.65 \pm 0.29\ \mu\text{g m}^{-3}$ ) and  $<0.14$  to  $-3.5\ \mu\text{g m}^{-3}$  (mean:  $1.43 \pm 0.73\ \mu\text{g m}^{-3}$ ), respectively (Figure 2a). These concentrations are broadly in the same range as previously reported concentrations at MCOH during dry winter, of EC,  $0.2\text{--}1.2\ \mu\text{g m}^{-3}$  [Gustafsson *et al.*, 2009],  $0.6 \pm 0.1\ \mu\text{g m}^{-3}$  [Stone *et al.*, 2012] and TC,  $1.5\ \mu\text{g m}^{-3}$  [Sheesley *et al.*, 2012]. The WSOC concentrations in  $PM_{2.5}$  ranged from 0.15 to 1.7 (mean:  $0.64 \pm 0.51\ \mu\text{g m}^{-3}$ ) and contributed 15–52% (mean:  $36 \pm 11\%$ ) of TC and 20–99% (mean:  $62 \pm 19\%$ ) of OC (Figures 2a and 4a). These concentrations are in accordance with reported concentrations of WSOC at MCOH [Kirillova *et al.*, 2013],  $0.52\ \mu\text{g m}^{-3}$  in TSP aerosols, which accounted for 25% of TC. The absolute WSOC concentrations at MCOH were expectedly much lower than those for fine aerosols in the source regions during wintertime,  $22 \pm 12\ \mu\text{g m}^{-3}$  in Delhi [Kirillova *et al.*, 2014a],  $7.5 \pm 0.10\ \mu\text{g m}^{-3}$  in Ahmedabad, western India [Rengarajan *et al.*, 2011], and  $21.3 \pm 9.3\ \mu\text{g m}^{-3}$  in Kanpur [Ram *et al.*, 2012].

During the course of the CARDEX campaign, three different periods could also be observed for the carbonaceous aerosol loadings. The highest concentrations were observed during the first 9 days of the campaign associated with air masses from IGP and Bay of Bengal (Period I,  $2.21 \pm 0.56\ \mu\text{g m}^{-3}$  and  $1.07 \pm 0.71\ \mu\text{g m}^{-3}$ , for TC and WSOC, respectively). A second period characterized by low carbonaceous aerosol loadings (Period II,  $TC = 0.88 \pm 0.50\ \mu\text{g m}^{-3}$ ,  $WSOC = 0.30 \pm 0.32\ \mu\text{g m}^{-3}$ ) during the next 17 days with air masses mainly coming from Arabian Sea and South Bay of Bengal, where low CA loadings were presumably associated with marine source air masses. Finally, a third period, with air masses originating closer to the receptor, with higher concentrations again (Period III,  $TC = 1.61 \pm 0.39\ \mu\text{g m}^{-3}$ ,  $WSOC = 0.66 \pm 0.19\ \mu\text{g m}^{-3}$ ).

The OC to EC ratios are affected by both emission source variability and processing during long-range transport. OC to EC ratios during CARDEX were  $1.2 \pm 0.5$ , which is accordance to previous studies at MCOH and similar to the few other reports available for tropical Asian sites dominated by long-range transport [Rajput *et al.*, 2014]. The OC/EC ratios at MCOH were lower than those from South Asian source regions. Coarse aerosols from Mumbai (India) and Dhaka (Bangladesh) during wintertime had OC/EC ratios of 2.0–3.2 [Venkataraman *et al.*, 2002] and 2.1 [Salam *et al.*, 2003], respectively. Fine Indian aerosols showed even higher OC/EC ratios, 5.0 in Delhi [Tiwari *et al.*, 2013], 7.1 in a suburban Indian site influenced by biogenic emissions [Pachauri *et al.*, 2013], and  $7.0 \pm 2.0$  for a downwind site in IGP [Srinivas and Sarin, 2014]. The aerosol source to receptor transport may lead to photochemical aging, differential washout or secondary organic aerosol (SOA) formation and consequently an increase or decrease of this ratio. A decrease of OC/EC ratio from source to receptor was also reported for the East Asia outflow [Lim *et al.*, 2003]. The OC/EC ratio decreased from source regions of China and Japan to increasing distance over Pacific, pointing out a shorter residence time in the marine atmosphere for OC than for EC. EC is a nonvolatile and very stable species, whereas OC contains either many semivolatile species that partition between gas and particle or polar compounds that are preferentially washed out [Granat *et al.*, 2010]. During long-range transport from source regions to regional sites, air is diluted with clean air and some particulate organic compounds may evaporate. Furthermore, the ratio of OC/EC during CARDEX did not show any significant diurnal change when comparing daytime and nighttime samples, suggesting that MCOH aerosols were not affected by local photochemical processes such as SOA formation, and instead, they were already aged.

Water-soluble organic carbon (WSOC) was a large portion of total carbonaceous aerosols (TC) during CARDEX. The fraction of WSOC in OC was highest for Periods I and III when air masses were influenced by pollution from the densely populated IGP ( $72 \pm 20\%$ ) and South India ( $66 \pm 12\%$ ), respectively. In contrast, the proportion of WSOC in OC was lower during Period II when air masses were mainly coming from the Arabian Sea ( $43 \pm 24\%$ ). WSOC contribution to OC at MCOH ( $62 \pm 19\%$ ) was somewhat higher than what has so far been reported for South Asian source regions ( $41 \pm 6\%$  in Ahmedabad [Rengarajan *et al.*, 2011] and  $48 \pm 13\%$  in Kanpur [Ram *et al.*, 2012]), suggesting that photochemical aging of OC during long-range transport of aerosols may lead to more oxygenated and thus water-soluble compounds [Aggarwal and Kawamura, 2009]. The same trend was observed in the work by Srinivas and Sarin [2013] for aerosols transported from the IGP ( $52 \pm 16\%$ ) to over the Bay of Bengal ( $77 \pm 10\%$ ).

### 3.3. Source Apportionment and Aerosol Processing by Dual Carbon Isotopes

Natural abundance radiocarbon ( $\Delta^{14}\text{C}$ ) analysis was applied to discern between fossil fuel versus biogenic emissions and biomass combustion sources of the different aerosol carbon components studied during

CARDEX. In PM<sub>2.5</sub> aerosols,  $\Delta^{14}\text{C}$  measurements showed the EC component to have the largest fossil fuel contribution (36–47%,  $41 \pm 4\%$ ) (Figure 2b). This was at the low end compared to what had been found in previous studies at MCOH ( $58 \pm 4\%$  (radiocarbon analysis [Gustafsson *et al.*, 2009]) and 40–50% (positive matrix factorization by multiple elements [Stone *et al.*, 2007])). In any case, the fossil fuel contribution to EC in the South Asian outflow is lower than in the East Asian outflow ( $76 \pm 5\%$  [Chen *et al.*, 2013] and 78% [Liu *et al.*, 2013a]). The  $^{14}\text{C}$ -fingerprinting further constrained that aerosol TOC stemmed 25–41% from fossil C stocks (mean:  $31 \pm 5\%$ ) while also the WSOC had a sizeable fossil C origin (8–22%, mean:  $14 \pm 5\%$ ) (Figure 2b). Despite substantial variations in overall carbon aerosol concentrations during the CARDEX campaign, there was little variation in observed  $\Delta^{14}\text{C}$  signal for any aerosol C fraction. This suggests rather constant relative contribution among different sources and formation pathways, illustrating the benefit of a pristine and remote recipient location such as MCOH in affording a large-scale integrating picture. Low  $^{14}\text{C}$ -fossil contributions to WSOC have been reported by several other studies across different aerosol sizes (PM<sub>2.5</sub>, PM<sub>10</sub>, and TSP) and sites (fossil <12% [Kirillova *et al.*, 2010], 11–19% [Kirillova *et al.*, 2013], 14–29% [Kirillova *et al.*, 2014a], 4–24% [Szidat *et al.*, 2004], 19–33% [Weber *et al.*, 2007], and 0–25% [Wozniak *et al.*, 2012]). It is worth noting that WSOC from the South Asian outflow has been found to have similar fossil fuel contribution compared to other sites in Europe and U.S. but lower than those from the East Asian outflow (12–49% fossil [Kirillova *et al.*, 2014b] and 19–45% fossil [Pavuluri *et al.*, 2013]). Given the absence of diurnal variability in WSOC/OC and OC/EC, it appears that the MCOH WSOC pool may be aged primary aerosols from biomass burning and secondary organic aerosols, also aged, from oxidation of VOC emissions from biomass burning and/or biogenic sources.

Specific inorganic elements in aerosols may also be used as indicators of sources. Non-sea-salt (NSS) sulfate ( $\text{SO}_4^{2-}$ ) is an indicator for fossil fuel combustion while potassium ( $\text{K}^+$ ) is found in plants and crustal dust, but much less in fossil fuels, and is thus used as a marker for biomass combustion [e.g., Novakov *et al.*, 2000].  $\text{K}^+$  to  $\text{SO}_4^{2-}$  and EC to  $\text{SO}_4^{2-}$  ratios were  $0.04 \pm 0.01$  and  $0.09 \pm 0.02$  during CARDEX (Figure S3). The two ratios correlate positively ( $R^2 = 0.71$ ). Higher ratios indicate a major influence of biomass burning sources. EC to  $\text{SO}_4^{2-}$  ratio at MCOH was observed higher than in an East Asian receptor (0.02–0.06, [Ramana *et al.*, 2010]), suggesting a substantial biofuel/biomass combustion contribution in South Asia. While  $\text{K}^+$  and  $\text{SO}_4^{2-}$  ratios may only be used as qualitative source tracers, the MCOH-CARDEX ratios are consistent with the more quantitative  $^{14}\text{C}$ -based source apportionment results.

Stable carbon isotope ( $\delta^{13}\text{C}$ ) analysis is informative for both source apportionment and particularly for atmospheric processing during long-range transport. Regarding sources, the  $\delta^{13}\text{C}$  for C<sub>4</sub> terrestrial vegetation (e.g., corn, sugar cane, grass; approximately  $-17$  to  $-9\%$ , mean  $-13\%$  [Smith and Epstein, 1971]), and marine (approximately  $-22$  to  $-18\%$  [Miyazaki *et al.*, 2011]) sources are enriched in  $^{13}\text{C}$  relative to C<sub>3</sub> terrestrial vegetation (wood; approximately  $-32$  to  $-20\%$ , mean  $27\%$  [Smith and Epstein, 1971]) and fossil fuel sources (coal approximately  $-24$  to  $-21\%$ , liquid fuel approximately  $-28$  to  $-24\%$ , and gas approximately  $-40$  to  $-28\%$  [Agnihotri *et al.*, 2011; Kawashima and Haneishi, 2012; Widory, 2006]). Some fractionation in  $\delta^{13}\text{C}$  may occur during incomplete combustion but this is at present poorly constrained [e.g., Currie *et al.*, 1999; Turekian *et al.*, 1998]. Importantly, studies have shown that atmospheric photochemical processes induce a fractionation in the aerosol  $\delta^{13}\text{C}$  due to the kinetic isotope effect (KIE; different reaction rates for  $^{12}\text{C}$  and  $^{13}\text{C}$  isotopes). For instance, aerosol photochemical aging leads to more positive  $\delta^{13}\text{C}$  values in the remaining aerosol [Aggarwal and Kawamura, 2008; Pavuluri and Kawamura, 2012], whereas SOA formation results in secondary compounds/aerosols that are depleted in  $^{13}\text{C}$  compared to the gaseous reactant(s) [Fisseha *et al.*, 2009b; Iannone *et al.*, 2010; Irei *et al.*, 2006; Miyazaki *et al.*, 2012] or compared to the leaf carbon for biogenic SOA [Rudolph *et al.*, 2003]. Hence, enrichment or depletion in  $\delta^{13}\text{C}$  is diagnostic for atmospheric processing of aerosols while their initial  $\delta^{13}\text{C}$  values depend on their sources [e.g., Kirillova *et al.*, 2013]. The CARDEX-PM<sub>2.5</sub>  $\delta^{13}\text{C}$  analysis showed WSOC to have substantially more positive signatures ( $-20.8 \pm 0.7\%$ ) compared to in EC ( $-25.8 \pm 0.3\%$ ) and in TOC ( $-25.3 \pm 0.7\%$ ). Similar to  $\Delta^{14}\text{C}$ , only very small  $\delta^{13}\text{C}$  variations were observed for any C aerosol component throughout the campaign (Figure 2c).

The dual effects of source apportionment and aerosol processing may be examined for the different components by combining  $\Delta^{14}\text{C}$  and  $\delta^{13}\text{C}$  data in the same plot, (Figure 3). EC, which has exclusively primary sources, had a MCOH-CARDEX  $\delta^{13}\text{C}$  signature which indicated contribution of both fossil fuel and C<sub>3</sub> biomass combustion ( $-25.8 \pm 0.3\%$ ). Based on the same  $\delta^{13}\text{C}$  value, input from C<sub>4</sub> vegetation burning or fractionation

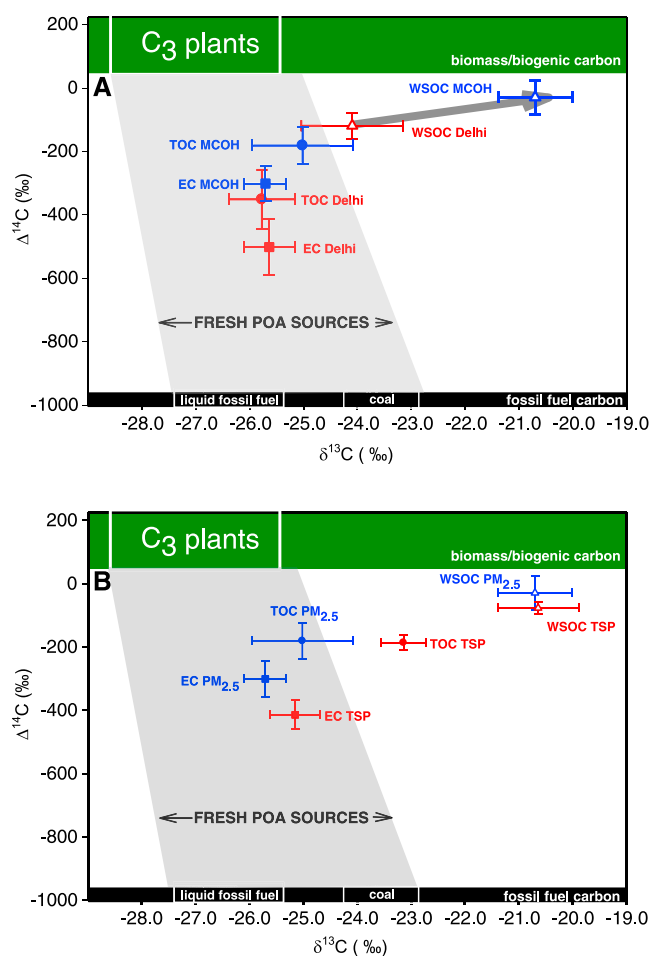


**Figure 3.** Two-dimensional dual carbon isotope  $\delta^{13}\text{C}$  versus  $\Delta^{14}\text{C}$  composition of several carbon aerosol fractions, (a) elemental carbon (EC, square), total organic carbon (TOC, circle), and water-soluble organic carbon (WSOC, triangle) in  $\text{PM}_{2.5}$  at MCOH during CARDEX campaign (blue) and Delhi during winter 2010–2011 (red) and (b) elemental carbon (EC, square), total organic carbon (TOC, circle), and water-soluble organic carbon (WSOC, triangle) in  $\text{PM}_{2.5}$  (blue) and TSP (red) at MCOH during CARDEX campaign. Symbols indicate mean of all measured samples and standard deviation as error bars. The dual-isotope signatures of fresh primary aerosol sources are marked in grey, considering  $\text{C}_3$  terrestrial vegetation, liquid, and solid fossil fuels as potential sources of carbonaceous aerosols at MCOH and Delhi.  $\delta^{13}\text{C}$  signatures on primary sources are based on reported literature values (coal  $(-23.6 \pm 0.7\text{‰})$ , liquid fossil  $(-26.4 \pm 1\text{‰})$ , and  $\text{C}_3$  vegetation  $(-27.0 \pm 1.6\text{‰})$ ) [Widory, 2006; Smith and Epstein, 1971]. The grey arrow in Figure 3a indicates  $^{13}\text{C}$  enrichment of WSOC during long-range transport from source to receptor sites.

WSOC compared to TC both in winter and summer seasons [Fisseha *et al.*, 2009a]. Molecular-specific isotope studies of dicarboxylic acids found an increase in  $\delta^{13}\text{C}$  values with a decrease in carbon numbers suggesting that shorter-chain diacids, which are formed by photochemical breakdown of longer-chain diacids, became  $^{13}\text{C}$  enriched because of the KIE effect [Aggarwal and Kawamura, 2008]. During atmospheric oxidation reactions, organic compounds break down to release  $\text{CO}_2/\text{CO}$ , whose isotopic composition would be  $^{13}\text{C}$  depleted, whereas the remaining aerosol OC/substrate becomes  $^{13}\text{C}$  enriched [Kirillova *et al.*, 2013; Wang and Kawamura, 2006; Wang *et al.*, 2010]. Whereas  $^{14}\text{C}$ -WSOC signature was similar between Delhi and MCOH, suggesting that WSOC is in both sites preferentially formed from modern rather than fossil fuel sources,  $^{13}\text{C}$ -WSOC values differed significantly ( $-20.8 \pm 0.7\text{‰}$  and  $-24.1 \pm 0.9\text{‰}$  for MCOH and Delhi, respectively).

during combustion processes may be ruled out. Combining isotopic data with other data on functional group composition and inorganic ratios from the same filter samples allowed excluding any significant contribution from marine sources during CARDEX. The ratios of non-sea-salt  $\text{SO}_4^{2-}$  and non-sea-salt  $\text{K}^+$  to total both  $\text{SO}_4^{2-}$  and  $\text{K}^+$  were  $98 \pm 1\%$  and  $93 \pm 4\%$ , respectively (Figure S3e). Hydroxyl functional groups accounted  $10 \pm 4\%$  of the total organic matter (OM) during CARDEX while for a marine-dominated aerosol region a contribution of 50% or more of OM is expected to be hydroxyl groups [Russell *et al.*, 2010] (Figure S3a).

Hence, assuming only minor contributions from marine and  $\text{C}_4$  vegetation sources, the enrichment in  $\delta^{13}\text{C}$  in WSOC compared to EC suggest a significant role for aerosol photochemical aging. Our previous studies in bulk TSP at MCOH and a West Indian receptor [Gustafsson *et al.*, 2009; Kirillova *et al.*, 2013] and in  $\text{PM}_{2.5}$  at an Indian source site [Kirillova *et al.*, 2014a] showed the same trend of enrichment in  $\delta^{13}\text{C}$ , and similarly, a less  $^{14}\text{C}$ -fossil WSOC compared to TOC and EC.

Comparing receptor (MCOH) and source (Delhi) sites for the same aerosol size in wintertime (Figure 3a, which includes Delhi data from Kirillova *et al.* [2014a]), longer distances/times of aerosol transportation apparently resulted in a growing offset in  $\delta^{13}\text{C}$  between WSOC and EC for sites further away from sources (i.e., the  $\Delta\delta^{13}\text{C}$  (WSOC-EC) was  $1.5\text{‰}$  for Delhi and  $5.0\text{‰}$  for MCOH). Other authors have also reported  $^{13}\text{C}$  enrichment during aerosol photochemical aging. Aerosols from Zurich city showed  $^{13}\text{C}$  enrichment in

This enrichment of  $^{13}\text{C}$  in WSOC at the receptor site clearly points to photochemical aging of aerosols during their long-range transport (Figure 3a).

Isotopic compositions in fine versus coarse fractions were also compared. Figure 3b compares isotopic signatures for EC, TOC, and WSOC components in both  $\text{PM}_{2.5}$  and TSP fractions. Three findings were made: (1) EC from TSP had a more fossil composition ( $50 \pm 4\%$ ) compared to EC from fine particles ( $41 \pm 4\%$ ). This may reflect a larger contribution of coal to the coarse fraction, which is also consistent with EC in TSP samples being slightly more  $\delta^{13}\text{C}$  enriched approaching the typical  $\delta^{13}\text{C}$  for coal combustion [Widory, 2006; Chen *et al.*, 2013]. (2) Similar  $\delta^{13}\text{C}$  and  $\Delta^{14}\text{C}$  signatures were observed for WSOC in both fractions, suggesting that nearly all WSOC is found in the fine fraction [Chalbot *et al.*, 2014] or in any case photochemical aging of WSOC during aerosol transport is happening to the same extent in both size fractions. (3) TOC from TSP is much more  $^{13}\text{C}$  enriched than TOC from  $\text{PM}_{2.5}$ , partly due to EC but also due to the remaining not-measured component, the nonwater-soluble organic carbon (NWSOC). Isotopic composition of NWSOC (NWSOC = TOC - WSOC - EC) was derived from WSOC, TOC, and EC data using an isotope mass balance equation similar to Kirillova *et al.* [2013]. These data are presented at supporting information (Figure S5). Large  $^{13}\text{C}$ -NWSOC differences were observed between both fractions. A  $\delta^{13}\text{C}$ -NWSOC depleted signature was observed in fine aerosols compared to  $\delta^{13}\text{C}$ -NWSOC in TSP. This  $\delta^{13}\text{C}$ -NWSOC shift between aerosol size fractions may be due to a predominance of SOA in the fine fraction rather in the coarse fraction.

### 3.4. Light Absorption of Water-Soluble Brown Carbon in the South Asian Outflow

Water-soluble Brown Carbon (WS-BrC) during CARDEX exhibited strong wavelength dependence, corroborating that WSOC is constituted of functional groups that, in contrast to BC, are light absorbing predominantly near ultraviolet wavelengths.  $\text{AAE}_{330-400\text{nm}}$  ranged from 6.1 to 9.5 ( $7.2 \pm 0.7$ , Figure 4c) and little variation was observed over time. This similarity suggests similar sources and chemical composition throughout the campaign, also consistent with the small variation in  $\delta^{13}\text{C}$  and  $\Delta^{14}\text{C}$  signatures. Other authors have reported similar AAE values for WS-BrC aerosols worldwide, 7.5 and 7.1 for Beijing winter and summer, respectively [Cheng *et al.*, 2011],  $6.4 \pm 0.6$  for the outflow from northern China intercepted over SE Yellow Sea [Kirillova *et al.*, 2014b], 6–7 for humic-like substances (HULIS) from Amazonia [Hoffer *et al.*, 2006], 6.2 to 8.3 [Hecobian *et al.*, 2010] and  $7.6 \pm 0.5$  [Zhang *et al.*, 2013] both for SE United States cities,  $5.1 \pm 2.0$  for Delhi [Kirillova *et al.*, 2014a], and  $6.0 \pm 1.1$  for a downwind site in IGP [Srinivas and Sarin, 2014] (Table S4).

Mass absorption cross section (MAC) measured at 365 nm was  $0.46 \pm 0.18 \text{ m}^2 \text{ g}^{-1}$  ( $0.26\text{--}0.88 \text{ m}^2 \text{ g}^{-1}$ ; Figure 4c), with little changes over time except for the beginning of Period II ( $0.78\text{--}0.88 \text{ m}^2 \text{ g}^{-1}$ ).  $\text{MAC}_{365}$  during CARDEX was lower than 1.79 and  $0.71 \text{ m}^2 \text{ g}^{-1}$  for Beijing winter and summer [Cheng *et al.*, 2011],  $1.6 \pm 0.5 \text{ m}^2 \text{ g}^{-1}$  for Delhi [Kirillova *et al.*, 2014a],  $0.7 \pm 0.2 \text{ m}^2 \text{ g}^{-1}$  for the East Asia outflow [Kirillova *et al.*, 2014b],  $0.70\text{--}0.73 \text{ m}^2 \text{ g}^{-1}$  for Los Angeles [Zhang *et al.*, 2013], and  $0.78 \pm 0.24 \text{ m}^2 \text{ g}^{-1}$  for a downwind site in IGP [Srinivas and Sarin, 2014] but similar to  $0.33 \text{ m}^2 \text{ g}^{-1}$  for Atlanta, SE United States [Zhang *et al.*, 2011],  $0.45 \pm 0.18 \text{ m}^2 \text{ g}^{-1}$  over the northern Indian Ocean [Srinivas and Sarin, 2013], and 0.29 and  $0.62 \text{ m}^2 \text{ g}^{-1}$  for rural sites in Georgia in summer and winter, respectively [Hecobian *et al.*, 2010] (Table S4). A detailed comparison of AAE and MAC values between this study and reported literature using the same water extraction method was conducted and is included in the supporting information (Figure S4b).

MAC values from different BrC sources, from both primary (POA) and secondary (SOA) origins, have been derived from laboratory experiments [Chen and Bond, 2010; Hoffer *et al.*, 2006; Kirchstetter and Novakov, 2004; Lambe *et al.*, 2013] (see Figure S4A). Primary BrC emitted from biomass burning appears to be more light absorptive than secondary aerosols, either anthropogenic or biogenic, i.e., MAC values at 405 nm range from  $0.18$  to  $1.5 \text{ m}^2 \text{ g}^{-1}$  for humic and fulvic acids [Lambe *et al.*, 2013], from  $0.13$  to  $1.1 \text{ m}^2 \text{ g}^{-1}$  for primary biomass burning aerosols [Chen and Bond, 2010], and from  $0.001$  to  $0.088 \text{ m}^2 \text{ g}^{-1}$  for SOA [Lambe *et al.*, 2013]. Among SOA, those with higher aromaticity (mainly from anthropogenic sources) show a higher light-absorbing efficiency [Lambe *et al.*, 2013]. Ambient studies have reported similar findings, i.e., largely modern SOA observed in Atlanta during summertime are less light absorptive than fresh fossil anthropogenic SOA from Los Angeles [Zhang *et al.*, 2011]; WSOC from rural sites in Georgia was more absorptive in winter, when WSOC was mainly influenced by biomass burning, than in summer [Hecobian *et al.*, 2010].

The water-soluble component of BrC was relatively weakly light absorbing relative to EC during CARDEX. There are different explanations in order to understand the lower light absorbance by WSOC at the receptor

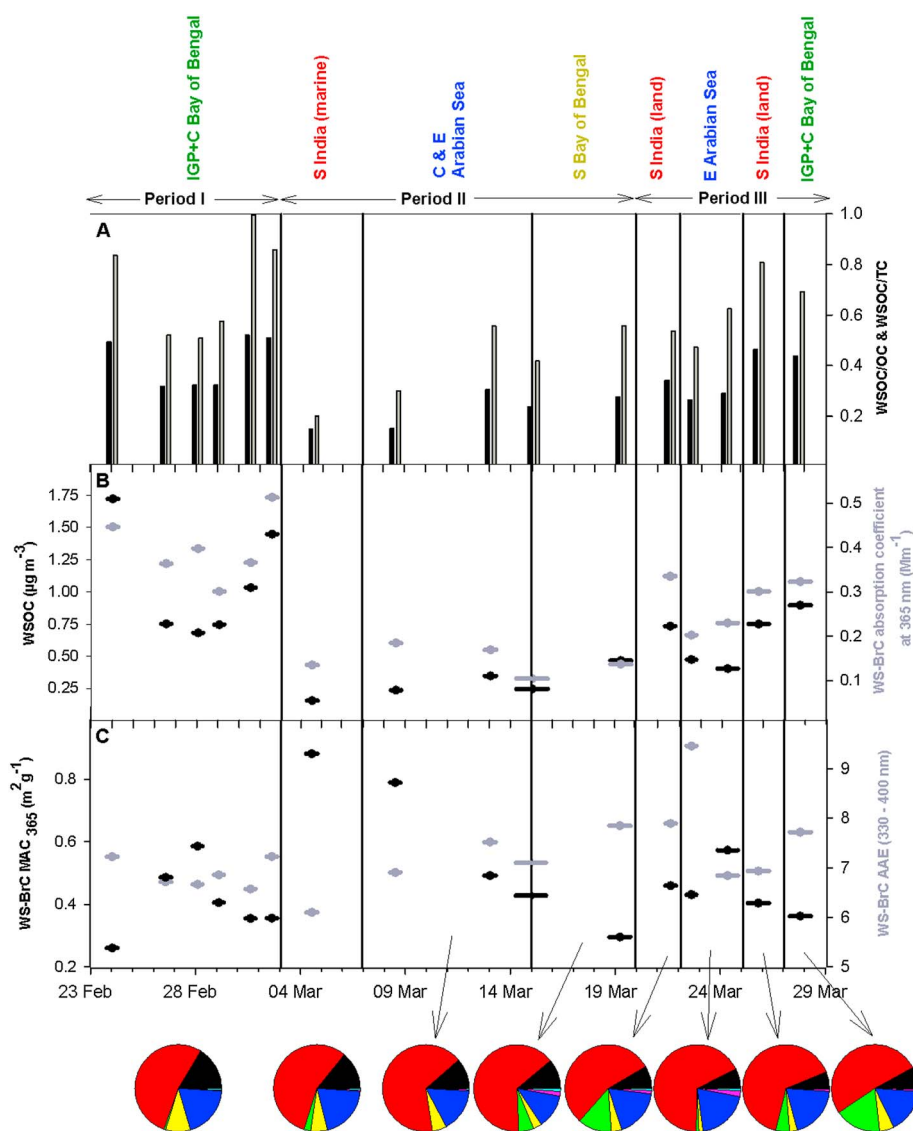


**Figure 4.** (a) WSOC to total carbon (TC, black) and WSOC to organic carbon (OC, grey) ratios; (b) water-soluble organic carbon (WSOC) concentrations and absorption coefficient at 365 nm of WS-BrC; and (c) mass absorption cross section (MAC) of water-soluble brown carbon (WS-BrC) at 365 nm and Absorption Ångström Exponent (AAE<sub>330-400nm</sub>) of WS-BrC in PM<sub>2.5</sub> at MCOH during CARDEX campaign. Back trajectory source clusters are marked at the top. FTIR composition for each source cluster is depicted at the bottom: alcohol (black), alkane (red), carbonyl (green), amine (yellow), carboxylic acid (dark blue), organosulfate (pink), and organonitrate (light blue). Fossil fuel combustion: alkanes, alcohols, and carboxylic acids are associated to fossil fuel combustion and nonacid carbonyls to biogenic and biomass combustion.

(MCOH;  $\text{MAC} = 0.5 \pm 0.2 \text{ m}^2 \text{g}^{-1}$ ) than in the source region (e.g., Delhi;  $\text{MAC} = 1.6 \pm 0.5 \text{ m}^2 \text{g}^{-1}$ , [Kirillova et al., 2014a]). These possible explanations are the following: (a) WSOC has a larger anthropogenic fossil contribution in the near-source than in the receptor site. Srinivas and Sarin [2013] recently published a similar observed decrease of MAC from IGP to over Bay of Bengal and they suggested that the source contribution to WSOC may be more anthropogenic at IGP than over Indian Ocean. This hypothesis can be ruled out here because very similar <sup>14</sup>C-WSOC values have been observed in the present study between MCOH and Delhi (see section 3.3). (b) Different origins of modern-WSOC between near-source and receptor sites. Modern-WSOC at Delhi might be predominantly from primary biomass burning aerosols, whereas modern-WSOC at MCOH might be composed of terrestrial-biogenic SOA or SOA formed over the ocean. Marine-related SOA at MCOH are unlikely to be present as the low Na<sup>+</sup> concentrations indicated (see section 3.3) and fresh biogenic SOA is not likely because the ratio OC to EC does not show any diurnal change (see section 3.2).

(c) Photochemical aging of WS-BrC during long-range transport leads to less absorptive chemical compounds. Both laboratory and field measurements have shown changes on aerosol absorption during photochemical aging, with aged OC being less absorptive than fresh OC [Zhong and Jang, 2014; Adler *et al.*, 2011]. (d) Photochemical aging leading to the mixture of WS-BrC with newly formed nonabsorbing WSOC during atmospheric transport, e.g., short-chain dicarboxylic acids. (e) A drift of the BrC component from water-soluble to water-insoluble forms during atmospheric transport. Water-insoluble carbonaceous spherules with strong absorbing carbon (tar balls) have been identified in aged biomass smoke [Alexander *et al.*, 2008; Pósfai *et al.*, 2004;]. Furthermore, methanol extracts of wood smoke and ambient aerosols have shown absorptive capacities greater than water extracts, sometimes of several orders of magnitude [Chen and Bond, 2010; Liu *et al.*, 2013b; Zhang *et al.*, 2013]. Taken together, it is first suggested that wintertime WSOC intercepted over the Indian receptor is an aged aerosol, stemming from primary biomass burning, possibly in combination with aged secondary aerosols from primary VOC emissions from biomass burning and terrestrial-biogenic sources. Second, constrained  $MAC_{365}$  values of the light-absorbing WSOC demonstrate a less absorbing WSOC aerosol over this Indian Ocean site than reported from sites closer to sources (Delhi/IGP) and/or in East Asia due to atmospheric aging processes which probably induce bleaching of chromophores, but also mixture with nonabsorbing WSOC components and WS-BrC drifting to a more water-insoluble BrC component.

### 3.5. Fractional Solar Radiation Absorbed by Water-Soluble Brown Carbon Relative to Elemental Carbon

A simplistic absorption-based calculation was employed to estimate the amount of solar energy absorbed by WS-BrC relative to elemental carbon (EC) at ground level at MCOH (see section 2.6). This fraction was during CARDEX small at  $0.7 \pm 0.2\%$ , whereas WS-BrC has been observed as a potential contributor to the global climate warming with relative high absorbing capacity of 2–10% in the East Asian outflow [Kirillova *et al.*, 2014b] and 3–11% in Delhi [Kirillova *et al.*, 2014a] using the same method as in the present study.

The absorbance contribution of BrC has been recently reported and investigated using different methods (see supporting information, Table S4 and Figure S4). Some studies are based on observational optical data and make specific assumptions regarding the optical properties of the components [Bahadur *et al.*, 2012; Chung *et al.*, 2012; Feng *et al.*, 2013]. For instance, BrC absorbance contribution, inferred from solar spectral observations of the column and in situ optical observations of ambient aerosols, is up to 20% of the total absorption by anthropogenic aerosols [Feng *et al.*, 2013]. Other studies are based on absorbance measurements from liquid extracts after filter extraction in water or organic solvents [Chen and Bond, 2010; Cheng *et al.*, 2011; Hoffer *et al.*, 2006; Kirillova *et al.*, 2014a, 2014b] reporting also significant BrC contributions to light absorption. Regarding this latter type of studies, Liu *et al.* [2013b] estimated the absorption of BrC based on Mie calculations from direct size-resolved measurements of chromophores in aerosol liquid extracts. The predicted BrC light absorption for ambient aerosol was a factor of 2 higher than light absorption in extracts. However, it is presently not clear how general this relation is for, e.g., samples collected in regions with a different source emission profile and dependence on long-range transport. Our estimate for the absorbance contribution of WS-BrC relative to EC is based on several assumptions (see section 2.6), but a sensitivity analysis has showed that the finding of a relatively small absorbance role of the WS-BrC component relative to EC stands unaffected at MCOH even when these assumptions are not completely fulfilled (see supporting information).

The relative light-absorbing contribution of WS-BrC at MCOH was smaller than what has been observed at other sites. For instance, Hoffer *et al.* [2006] showed that WS-BrC from HULIS accounted for 6–9% of the total light absorption. Kirchstetter and Thatcher [2012] showed that OC in wood smoke accounted for 14% of the total light absorption by OC + BC (acetone-extracted filter-based method). There are mainly two factors which explain this fact: first, the low light-absorbing efficiency by WS-BrC at MCOH ( $MAC_{365}$ ) (see section 3.4) and second, low concentration ratio of WS-BrC to EC at MCOH compared to at other near-source sites. The former observation indicates influence by atmospheric processing during long-range transport, and the latter is likely due to the shorter atmospheric residence time of WS-BrC relative to EC [Lim *et al.*, 2003]. Another important point is that it has been suggested that a significant fraction of the light-absorbing OC (BrC) is relatively hydrophobic and is thus not extracted by water, indicating that the total absorbance contribution from BrC is expected to be higher [e.g., Liu *et al.*, 2013b; Psichoudaki and Pandis, 2013; Zhang *et al.*, 2013]. This fact is corroborated when comparing studies where the BrC absorption is derived from optical observations of OC (including both water-soluble and insoluble fractions) and the ones isolating only the water-soluble

component. For the first case, slightly higher BrC absorbance contributions are observed. Taken together, further investigations are needed to understand (a) atmospheric processes which may lead to less light-absorbing OC forms, i.e., mixing with other nonabsorbing constituents or other effects such as aerosol bleaching induced by photochemical reactions and (b) the absorbance contribution of the water-insoluble OC component of aerosols being this component the next target for further investigations on BrC.

#### 4. Conclusions

The high-intensity CARDEX campaign, held in February and March 2012 at the Maldives Climate Observatory on Hanimaadhoo (MCOH), a receptor for the pollutant South Asian outflow, addressed the semidirect aerosol effect, with sources, atmospheric processing, and light-absorbing properties of water-soluble organic carbon aerosols detailed in this report. This late wintertime period is related to high aerosol loadings at MCOH. Radiocarbon-based source diagnostics constrained the fossil contribution to  $14 \pm 5\%$  and  $41 \pm 4\%$  of the water-soluble organic carbon (WSOC) and elemental carbon (EC), respectively, which establishes a greater role for biogenic and biomass combustion source in the outflow from South Asia than in East Asia. No substantial variation in source apportionment and optical properties were distinguished among the different South Asian air mass origins. The combination of dual carbon isotopes for source apportionment and optical properties of the WSOC component suggests that wintertime WSOC intercepted over the Indian receptor is an aged aerosol, mainly stemming from biomass burning, and this aging may lead to less light-absorptive water-soluble compounds. Based on these results, the emerging need is to better constrain the sources of both water-soluble and water-insoluble brown carbon (BrC) since atmospheric reactions occurring during long-range transport may change the optical properties of BrC as well as the partitioning of BrC between the hydrophilic/hydrophobic components of aerosols.

#### Acknowledgments

The CARDEX field campaign was sponsored and funded by the National Science Foundation and conducted by the Scripps Institution of Oceanography at the University of California (San Diego, USA) in collaboration with the Desert Research Institute (Nevada, USA), Stockholm University (Stockholm, Sweden), and Max Planck Institute (Hamburg, Germany). V. Ramanathan was the principal investigator of CARDEX, E. Wilcox was the Co-PI, and H. Nguyen was the field director who conducted the campaign with full support by the Environmental Protection Agency of the Republic of Maldives. Full details of the CARDEX campaign can be found in: [http://www.ramanathan.ucsd.edu/files/CARDEX\\_prop\\_Jun\\_20.pdf](http://www.ramanathan.ucsd.edu/files/CARDEX_prop_Jun_20.pdf). This study is Paper#1 from the CARDEX campaign. The authors acknowledge financial support from the Swedish funding agencies FORMAS (214-2009-970), STEM (35450-2), and Sida (AKT-2010-038). C.B. acknowledges additional financial support from EU Marie Curie Programme (PIEF-GA-2011-198507). Ö.G. acknowledges financial support from the Knut and Alice Wallenberg Foundation. N.D.B. acknowledges financial support from NASA EPSCoR (NNX10AR89A) and by NASA ROSES (NNX11AB79G). This study also benefitted from the research environments provided by the Bolin Centre for Climate Research and the Delta Facility (a core facility for compound-specific isotope analysis), both at the Stockholm University and School of Natural Sciences. The data for Figure 1 are available at NOAA HYSPLIT software v4 (<http://www.arl.noaa.gov/ready/hysplit4.html>) and NASA MODIS Level 1 (<http://ladsweb.nascom.nasa.gov/index.html>). Data supporting Figures 2–4 are available as in supporting information Tables S1 and S5–S7. For further information regarding the data set, contact the author A. Andersson at the following e-mail address: [august.andersson@itm.su.se](mailto:august.andersson@itm.su.se). Finally, we would like to thank Moosmüller and Chakrabarty from Desert Research Institute (Reno, NV) for their advice and interpretation of IC data.

#### References

- Adler, G., J. M. Flores, A. Abo Rizeq, S. Borrmann, and Y. Rudich (2011), Chemical, physical, and optical evolution of biomass burning aerosols: A case study, *Atmos. Chem. Phys.*, *11*, 1491–1503.
- Aggarwal, S. G., and K. Kawamura (2008), Molecular distributions and stable carbon isotopic compositions of dicarboxylic acids and related compounds in aerosols from Sapporo, Japan: Implications for photochemical aging during long-range atmospheric transport, *J. Geophys. Res.*, *113*, D14301, doi:10.1029/2007JD009365.
- Aggarwal, S. G., and K. Kawamura (2009), Carbonaceous and inorganic composition in long-range transported aerosols over northern Japan: Implication for aging of water-soluble organic fraction, *Atmos. Environ.*, *43*, 2532–2540.
- Agnihotri, R., T. K. Mandal, S. G. Karapurkar, M. Naja, R. Gadi, Y. Nazeer Ahammmed, A. Kumar, T. Saud, and M. Saxena (2011), Stable carbon and nitrogen isotopic composition of bulk aerosols over India and northern Indian Ocean, *Atmos. Environ.*, *45*, 2828–2835.
- Alexander, D. T. L., P. A. Crozier, and J. R. Anderson (2008), Brown carbon spheres in East Asian outflow and their optical properties, *Science*, *321*, 833–836.
- Andersson, A. (2011), A systematic examination of a random sampling strategy for source apportionment calculations, *Sci. Total Environ.*, *412*, 232–238.
- Andreae, M. O., and A. Gelencser (2006), Black carbon or brown carbon? The nature of light-absorbing carbonaceous aerosols, *Atmos. Chem. Phys.*, *6*, 3131–3148.
- Bahadur, R., P. S. Praveen, Y. Xu, and V. Ramanathan (2012), Solar absorption by elemental and brown carbon determined from spectral observations, *Proc. Natl. Acad. Sci. U.S.A.*, *109*, 17,366–17,371.
- Birch, M. E., and R. A. Cary (1996), Elemental carbon-based method for monitoring occupational exposures to particulate diesel exhaust, *Aerosol Sci. Technol.*, *25*, 221–241.
- Bond, T. C., and R. W. Bergstrom (2006), Light absorption by carbonaceous particles: An investigative review, *Aerosol Sci. Technol.*, *40*, 27–67.
- Bond, T. C., et al. (2013), Bounding the role of black carbon in the climate system: A scientific assessment, *J. Geophys. Res. Atmos.*, *118*, 5380–5552, doi:10.1002/jgrd.50171.
- Brunekreef, B., and B. Forsberg (2005), Epidemiological evidence of effects of coarse airborne particles on health, *Eur. Respir. J.*, *26*, 309–318.
- Butler, O. T., W. R. L. Cairns, J. M. Cook, and C. M. Davidson (2009), Atomic spectrometry update. Environmental analysis, *J. Anal. At. Spectrom.*, *24*(2), 131–177.
- Chakrabarty, R. K., S. Pervez, J. C. Chow, J. G. Watson, S. Dewangan, J. Robles, and G. Tian (2014), Funeral pyres in India: Brown carbon aerosol emissions and climate impacts, *Environ. Sci. Technol. Lett.*, *1*(1), 44–48.
- Chalbot, M., J. Brown, P. Chitranshi, G. Gamboa da Costa, E. D. Pollock, and I. G. Kavouras (2014), Functional characterization of the water-soluble organic carbon of size-fractionated aerosol in the Southern Mississippi Valley, *Atmos. Chem. Phys.*, *14*, 6075–6088.
- Chen, Y., and T. C. Bond (2010), Light absorption by organic carbon from wood combustion, *Atmos. Chem. Phys.*, *10*, 1773–1787.
- Chen, B., et al. (2013), Source forensics of black carbon aerosols from China, *Environ. Sci. Technol.*, *47*, 9102–9108.
- Cheng, Y., et al. (2011), Mass absorption efficiency of elemental carbon and water-soluble organic carbon in Beijing, China, *Atmos. Chem. Phys.*, *11*, 11,497–11,510.
- Chow, J. C., and J. G. Watson (1999), Ion chromatography in elemental analysis of airborne particles, in *Elemental Analysis of Airborne Particles*, vol. 1, edited by S. Landsberger and M. Creatchman, pp. 97–137, Gordon and Breach Science, Amsterdam.
- Chung, C. E., V. Ramanathan, and D. Decremer (2012), Observationally constrained estimates of carbonaceous aerosol radiative forcing, *Proc. Natl. Acad. Sci. U.S.A.*, *109*, 11,624–11,629.

- Currie, L. A., G. A. Klouda, B. A. Benner Jr., K. Garrity, and T. I. Eglinton (1999), Isotopic and molecular fractionation in combustion; three routes to molecular marker validation, including direct molecular "dating" (GC/AMS), *Atmos. Environ.*, **33**, 2789–2806.
- Ding, X., X.-M. Wang, Q.-F. He, X.-X. Fu, and B. Gao (2013), Water-soluble organic carbon over the Pearl River Delta region during fall-winter: Spatial variations and source apportionment, *Atmos. Chem. Phys. Discuss.*, **13**, 13,773–13,798.
- Feng, Y., V. Ramanathan, and V. R. Kotamarthi (2013), Brown carbon: A significant atmospheric absorber of solar radiation?, *Atmos. Chem. Phys.*, **13**, 8607–8621.
- Fernandez, F. J. (1989), Atomic absorption spectroscopy, in *Methods of Air Sampling and Analysis*, edited by J. P. Lodge Jr., 3rd ed., pp. 83–89, Lewis, Chelsea, Mich.
- Fisseha, R., M. Saurer, M. Jäggi, R. T. W. Siegwolf, J. Dommen, S. Szidat, V. Samburova, and U. Baltensperger (2009a), Determination of primary and secondary sources of organic acids and carbonaceous aerosols using stable carbon isotopes, *Atmos. Environ.*, **43**, 431–437.
- Fisseha, R., H. Spahn, R. Wegener, T. Hohaus, G. Brasse, H. Wissel, R. Tillmann, A. Wahner, R. Koppmann, and A. Kiendler-Scharr (2009b), Stable carbon isotope composition of secondary organic aerosol from beta-pinene oxidation, *J. Geophys. Res.*, **114**, D02304, doi:10.1029/2008JD011326.
- Fung, K. K., et al. (1979), Comparison of ion chromatography and automated wet chemical methods for analysis of sulfate and nitrate in ambient particulate filter samples, in *Ion Chromatographic Analysis of Environmental Pollutants*, edited by E. Sawicki and J. D. Mulik, pp. 203–209, Ann Arbor Sci. Inc., Ann Arbor, Mich.
- Gilardoni, S., et al. (2007), Regional variation of organic functional groups in aerosol particles on four US east coast platforms during the International Consortium for Atmospheric Research on Transport and Transformation 2004 campaign, *J. Geophys. Res.*, **112**, D10S27, doi:10.1029/2006JD007737.
- Granat, L., J. E. Engström, S. Praveen, and H. Rodhe (2010), Light absorbing material (soot) in rain water and in aerosol particles in the Maldives, *J. Geophys. Res.*, **115**, D16307, doi:10.1029/2009JD013768.
- Graven, H. D., T. P. Guilderson, and R. F. Keeling (2012), Observations of radiocarbon in CO<sub>2</sub> at seven global sampling sites in the Scripps flask network: Analysis of spatial gradients and seasonal cycles, *J. Geophys. Res.*, **117**, D02303, doi:10.1029/2011JD016535.
- Gustafsson, O., M. Kruså, Z. Zencak, R. J. Sheesley, L. Granat, E. Engström, P. S. Praveen, P. S. Rao, C. Leck, and H. Rodhe (2009), Brown clouds over South Asia: Biomass or fossil fuel combustion?, *Science*, **323**, 495–498.
- Hecobian, A., X. Zhang, M. Zheng, N. Frank, E. S. Edgerton, and R. J. Weber (2010), Water-soluble organic aerosol material and the light-absorption characteristics of aqueous extracts measured over the Southeastern United States, *Atmos. Chem. Phys.*, **10**, 5965–5977.
- Hoffer, A., A. Gelencsér, P. Guyon, G. Kiss, O. Schmid, G. P. Frank, P. Artaxo, and M. O. Andreae (2006), Optical properties of humic-like substances (HULIS) in biomass-burning aerosols, *Atmos. Chem. Phys.*, **6**, 3563–3570.
- Iannone, R., R. Koppmann, and J. Rudolph (2010), Stable carbon kinetic isotope effects for the production of methacrolein and methyl vinyl ketone from the gas-phase reactions of isoprene with ozone and hydroxyl radicals, *Atmos. Environ.*, **44**, 4135–4141.
- Irei, S., L. Huang, F. Collin, W. Zhang, D. Hastie, and J. Rudolph (2006), Flow reactor studies of the stable carbon isotope composition of secondary particulate organic matter generated by OH-radical-induced reactions of toluene, *Atmos. Environ.*, **40**, 5858–5867.
- Jacobson, M. Z. (1999), Isolating nitrated and aromatic aerosols and nitrated aromatic gases as sources of ultraviolet light absorption, *J. Geophys. Res.*, **104**, 3527–3542, doi:10.1029/1998JD100054.
- Jacobson, M. Z. (2012), Investigating cloud absorption effects: Global absorption properties of black carbon, tar balls, and soil dust in clouds and aerosols, *J. Geophys. Res.*, **117**, D06205, doi:10.1029/2011JD017218.
- Kawashima, H., and Y. Haneishi (2012), Effects of combustion emissions from the Eurasian continent in winter on seasonal delta C-13 of elemental carbon in aerosols in Japan, *Atmos. Environ.*, **46**, 568–579.
- Kirchstetter, T. W., and T. Novakov (2004), Evidence that the spectral dependence of light absorption by aerosols is affected by organic carbon, *J. Geophys. Res.*, **109**, D21208, doi:10.1029/2004JD004999.
- Kirchstetter, T. W., and T. L. Thatcher (2012), Contribution of organic carbon to wood smoke particulate matter absorption of solar radiation, *Atmos. Chem. Phys.*, **12**, 6067–6072.
- Kirillova, E. N., R. J. Sheesley, A. Andersson, and Ö. Gustafsson (2010), Natural abundance <sup>13</sup>C and <sup>14</sup>C analysis of water-soluble organic carbon in atmospheric aerosols, *Anal. Chem.*, **82**, 7973–7978.
- Kirillova, E. N., A. Andersson, R. J. Sheesley, M. Kruså, P. S. Praveen, K. Budhavant, P. D. Safai, P. S. P. Rao, and Ö. Gustafsson (2013), <sup>13</sup>C- and <sup>14</sup>C-based study of sources and atmospheric processing of water-soluble organic carbon (WSOC) in South Asian aerosols, *J. Geophys. Res.*, **118**, 614–626, doi:10.1002/jgrd.50130.
- Kirillova, E. N., A. Andersson, S. Tiwari, A. K. Srivastava, D. S. Bisht, and Ö. Gustafsson (2014a), Water-soluble organic carbon aerosols during a full New Delhi winter: Isotope-based source apportionment and optical properties, *J. Geophys. Res. Atmos.*, **119**, 3476–3485, doi:10.1002/2013JD020041.
- Kirillova, E. N., A. Andersson, J. Han, M. Lee, and Ö. Gustafsson (2014b), Sources and light absorption of water-soluble organic carbon aerosols in the outflow from northern China, *Atmos. Chem. Phys.*, **14**, 1413–1422.
- Klinedinst, D. B., and L. A. Currie (1999), Direct quantification of PM<sub>2.5</sub> fossil and biomass carbon within the northern front range air quality study's domain, *Environ. Sci. Technol.*, **33**, 4146–4154.
- Lambe, A. T., et al. (2013), Relationship between oxidation level and optical properties of secondary organic aerosol, *Environ. Sci. Technol.*, **47**, 6349–6357.
- Lawrence, M. G., and J. Lelieveld (2010), Atmospheric pollutant outflow from southern Asia: A review, *Atmos. Chem. Phys.*, **10**, 11,017–11,096.
- Levinson, R., H. Akbari, and P. Berdahl (2010), Measuring solar reflectance—Part I: Defining a metric that accurately predicts solar heat gain, *Sol. Energy*, **84**, 1717–1744.
- Lim, H. J., B. J. Turpin, L. M. Russell, and T. S. Bates (2003), Organic and elemental carbon measurements during ACE-Asia suggest a longer atmospheric lifetime for elemental carbon, *Environ. Sci. Technol.*, **37**, 3055–3061.
- Liu, D., J. Li, Y. Zhang, Yue Xu, X. Liu, P. Ding, C. Shen, Y. Chen, C. Tian, and G. Zhang (2013a), The use of levoglucosan and radiocarbon for source apportionment of PM<sub>2.5</sub> carbonaceous aerosols at a background site in east China, *Environ. Sci. Technol.*, **47**, 10,454–10,461.
- Liu, J., M. Bergin, H. Guo, L. King, N. Kotra, E. Edgerton, and R. J. Weber (2013b), Size-resolved measurements of brown carbon in water and methanol extracts and estimates of their contribution to ambient fine-particle light absorption, *Atmos. Chem. Phys.*, **13**, 12,389–12,404.
- Liu, J., et al. (2014), Brown carbon in the continental troposphere, *Geophys. Res. Lett.*, **41**, 2191–2195, doi:10.1002/2013GL058976.
- McNichol, A. P., A. R. Gagnon, G. A. Jones, and E. A. Osborne (1992), Illumination of a black box—Analysis of gas-composition during graphite target preparation, *Radiocarbon*, **34**, 321–329.
- Miyazaki, Y., K. Kawamura, J. Jung, H. Furutani, and M. Uematsu (2011), Latitudinal distributions of organic nitrogen and organic carbon in marine aerosols over the western North Pacific, *Atmos. Chem. Phys.*, **11**, 3037–3049.
- Miyazaki, Y., P. Q. Fu, K. Kawamura, Y. Mizoguchi, and K. Yamanoi (2012), Seasonal variations of stable carbon isotopic composition and biogenic tracer compounds of water-soluble organic aerosols in a deciduous forest, *Atmos. Chem. Phys.*, **12**, 1367–1376.

- Mohr, C., et al. (2013), Contribution of nitrated phenols to wood burning brown carbon light absorption in Detling, United Kingdom during winter time, *Environ. Sci. Technol.*, *47*, 6316–6324.
- Moosmüller, H., R. K. Chakrabarty, K. M. Ehlers, and W. P. Arnott (2011), Absorption Angstrom coefficient, brown carbon, and aerosols: Basic concepts, bulk matter, and spherical particles, *Atmos. Chem. Phys.*, *11*, 1217–1225.
- Novakov, T., M. O. Andreae, R. Gabriel, T. W. Kirchstetter, O. L. Mayol-Bracero, and V. Ramanathan (2000), Origin of carbonaceous aerosols over the tropical Indian Ocean: Biomass burning or fossil fuels?, *Geophys. Res. Lett.*, *27*, 4061–4064, doi:10.1029/2000GL011759.
- Pachauri, T., V. Singla, A. Satsangi, A. Lakhani, and K. Maharaj Kumari (2013), Characterization of carbonaceous aerosols with special reference to episodic events at Agra, India, *Atmos. Res.*, *128*, 98–110.
- Pavuluri, C. M., and K. Kawamura (2012), Evidence for 13-carbon enrichment in oxalic acid via iron catalyzed photolysis in aqueous phase, *Geophys. Res. Lett.*, *39*, L03802, doi:10.1029/2011GL050398.
- Pavuluri, C. M., K. Kawamura, M. Uchida, M. Kondo, and P. Fu (2013), Enhanced modern carbon and biogenic organic tracers in Northeast Asian aerosols during spring/summer, *J. Geophys. Res. Atmos.*, *118*, 2362–2371, doi:10.1002/jgrd.50244.
- Pearson, A., A. P. McNichol, R. J. Schneider, K. F. von Reden, and Y. Zheng (1998), Microscale AMS C-14 measurement at NOSAMS, *Radiocarbon*, *40*, 61–75.
- Pósfai, M., A. Gelencsér, R. Simonics, K. Arató, J. Li, P. V. Hobbs, and P. R. Buseck (2004), Atmospheric tar balls: Particles from biomass and biofuel burning, *J. Geophys. Res.*, *109*, D06213, doi:10.1029/2003JD004169.
- Psichoudaki, M., and S. N. Pandis (2013), Atmospheric aerosol water-soluble organic carbon measurement: A theoretical analysis, *Environ. Sci. Technol.*, *47*, 9791–9798.
- Rajput, P., M. Sarin, D. Sharma, and D. Singh (2014), Characteristics and emission budget of carbonaceous species from post-harvest agricultural-waste burning in source region of the Indo-Gangetic Plain, *Tellus Ser. B Chem. Phys. Meteorol.*, *66*, 21026, doi:10.3402/tellusb.v66.21026.
- Ram, K., M. M. Sarin, and S. N. Tripathi (2012), Temporal trends in atmospheric PM<sub>2.5</sub>, PM<sub>10</sub>, elemental carbon, organic carbon, water-soluble organic carbon, and optical properties: Impact of biomass burning emissions in the Indo-Gangetic Plain, *Environ. Sci. Technol.*, *46*, 686–695.
- Ramana, M. V., V. Ramanathan, Y. Feng, S.-C. Yoon, S.-W. Kim, G. R. Carmichael, and J. J. Schauer (2010), Warming influenced by the ratio of black carbon to sulphate and the black-carbon source, *Nat. Geosci.*, *3*, 542–545.
- Ramanathan, V., and G. Carmichael (2008), Global and regional climate changes due to black carbon, *Nat. Geosci.*, *1*, 221–227.
- Ramanathan, V., et al. (2001), Indian Ocean Experiment: An integrated analysis of the climate forcing and effects of the great Indo-Asian haze, *J. Geophys. Res.*, *106*(D22), 28,371–28,398, doi:10.1029/2001JD900133.
- Ramanathan, V., et al. (2007), Atmospheric brown clouds: Hemispherical and regional variations in long-range transport, absorption and radiative forcing, *J. Geophys. Res.*, *112*, D22S211, doi:10.1029/2006JD008124.
- Rengarajan, R., A. K. Sudheer, and M. M. Sarin (2011), Wintertime PM<sub>2.5</sub> and PM<sub>10</sub> carbonaceous and inorganic constituents from urban site in western India, *Atmos. Res.*, *102*, 420–431.
- Rhodes, J. R., et al. (1989), General atomic absorption procedure for trace metals, in *Methods of Air Sampling and Analysis*, edited by J. P. Lodge, pp. 608–618, Lewis Publishers, Inc., Chelsea, Mich.
- Rudolph, J., R. S. Anderson, K. V. Czapiewski, E. Czuba, D. Ernst, T. Gillespie, L. Huang, C. Rigby, and A. E. Thompson (2003), The stable carbon isotope ratio of biogenic emissions of isoprene and the potential use of stable isotope ratio measurements to study photochemical processing of isoprene in the atmosphere, *J. Atmos. Chem.*, *44*, 39–55.
- Russell, L. M., R. Bahadur, and P. J. Ziemann (2010), Identifying organic aerosol sources by comparing functional group composition in chamber and atmospheric particles, *Proc. Natl. Acad. Sci. U.S.A.*, *108*, 3516–3521.
- Salam, A., H. Bauer, K. Kassim, S. Mohammad Ullah, and H. Puxbaum (2003), Aerosol chemical characteristics of a mega-city in Southeast Asia (Dhaka-Bangladesh), *Atmos. Environ.*, *37*, 2517–2528.
- Saleh, R., C. J. Hennigan, G. R. McMeeking, W. K. Chuang, E. S. Robinson, H. Coe, N. M. Donahue, and A. L. Robinson (2013), Absorptivity of brown carbon in fresh and photo-chemically aged biomass-burning emissions, *Atmos. Chem. Phys.*, *13*, 7683–7693.
- Samset, B. H., and G. Myhre (2011), Vertical dependence of black carbon, sulphate and biomass burning aerosol radiative forcing, *Geophys. Res. Lett.*, *38*, L24802, doi:10.1029/2011GL049697.
- Sandell, E. B. (1959), *Colorimetric Determination of Traces of Metals*, John Wiley, New York.
- Sheesley, R. J., E. Kirillova, A. Andersson, M. Kruså, P. S. Praveen, K. B. Budhvant, P. Digambar Safai, P. S. P. Rao, and O. Gustafsson (2012), Year-round radiocarbon-based source apportionment of carbonaceous aerosols at two background sites in South Asia, *J. Geophys. Res.*, *117*, D10202, doi:10.1029/2011JD017161.
- Smith, B. N., and S. Epstein (1971), Two Categories of <sup>13</sup>C/<sup>12</sup>C Ratios for Higher Plants, *Plant Physiol.*, *47*(3), 380–384.
- Srinivas, B., and M. M. Sarin (2013), Light-absorbing organic aerosols (brown carbon) over the tropical Indian Ocean: Impact of biomass burning emissions, *Environ. Res. Lett.*, *8*, doi:10.1088/1748-9326/8/4/044042.
- Srinivas, B., and M. M. Sarin (2014), Brown carbon in atmospheric outflow from the Indo-Gangetic Plain: Mass absorption efficiency and temporal variability, *Atmos. Environ.*, *89*, 835–843.
- Stone, E. A., G. C. Lough, J. J. Schauer, P. S. Praveen, C. E. Corrigan, and V. Ramanathan (2007), Understanding the origin of black carbon in the atmospheric brown cloud over the Indian Ocean, *J. Geophys. Res.*, *112*, D22S23, doi:10.1029/2006JD008118.
- Stone, E. A., L. Yang, and L. E. Yu (2012), Characterization of organosulfates in atmospheric aerosols at Four Asian locations, *Atmos. Environ.*, *47*, 323–329.
- Sun, H. L., L. Biedermann, and T. C. Bond (2007), Color of brown carbon: A model for ultraviolet and visible light absorption by organic carbon aerosol, *Geophys. Res. Lett.*, *34*, L17813, doi:10.1029/2007GL029797.
- Szidat, S., et al. (2004), Source apportionment of aerosols by C-14 measurements in different carbonaceous particle fractions, *Radiocarbon*, *46*, 475–484.
- Takahama, S., A. Johnson, and L. M. Russell (2013), Quantification of carboxylic and carbonyl functional groups in organic aerosol infrared absorbance spectra, *Aerosol Sci. Technol.*, *47*, 310–325.
- Tiwari, S., A. Srivastava, D. Bisht, P. Safai, and P. Parmita (2013), Assessment of carbonaceous aerosol over Delhi in the Indo-Gangetic Basin: Characterization, sources and temporal variability, *Nat. Hazards*, *65*, 1745–1764.
- Turekian, V. C., S. Macko, D. Ballentine, R. J. Swap, and M. Garstang (1998), Causes of bulk carbon and nitrogen isotopic fractionations in the products of vegetation burns: Laboratory studies, *Chem. Geol.*, *152*, 181–192.
- Venkataraman, C., et al. (2002), Aerosol size and chemical characteristics at Mumbai, India, during the INDOEX-IPF (1999), *Atmos. Environ.*, *36*, 1979–1991.
- Wang, H. B., and K. Kawamura (2006), Stable carbon isotopic composition of low-molecular-weight dicarboxylic acids and ketoacids in remote marine aerosols, *J. Geophys. Res.*, *111*, D07304, doi:10.1029/2005JD006466.

- Wang, G., M. Xie, S. Hu, S. Gao, E. Tachibana, and K. Kawamura (2010), Dicarboxylic acids, metals and isotopic compositions of C and N in atmospheric aerosols from inland China: Implications for dust and coal burning emission and secondary aerosol formation, *Atmos. Chem. Phys.*, *10*, 6087–6096.
- Weber, R. J., et al. (2007), A study of secondary organic aerosol formation in the anthropogenic-influenced southeastern United States, *J. Geophys. Res.*, *112*, D13302, doi:10.1029/2007JD008408.
- WHO Air Quality Guidelines (2006), *Air Quality Guidelines for Particulate Matter, Ozone, Nitrogen Dioxide and Sulfur Dioxide*, World Health Organ., Geneva, Switzerland.
- Widory, D. (2006), Combustibles, fuels and their combustion products: A view through carbon isotopes, *Combust. Theory Modell.*, *10*, 831–841.
- Wozniak, A. S., J. E. Bauer, and R. M. Dickhut (2012), Characteristics of water-soluble organic carbon associated with aerosol particles in the eastern United States, *Atmos. Environ.*, *46*, 181–188.
- Zencak, Z., M. Elmquist, and Ö. Gustafsson (2007a), Quantification and radiocarbon source apportionment of black carbon in atmospheric aerosols using the CTO-375 method, *Atmos. Environ.*, *41*, 7895–7906.
- Zencak, Z., C. M. Reddy, E. L. Teuten, L. Xu, A. P. McNichol, and Ö. Gustafsson (2007b), Evaluation of gas chromatographic isotope fractionation and process contamination by carbon in compound-specific radiocarbon analysis, *Anal. Chem.*, *79*, 2042–2049.
- Zhang, Q., et al. (2009), Asian emissions in 2006 for the NASA INTEX-B mission, *Atmos. Chem. Phys.*, *9*, 5131–5153.
- Zhang, X. L., Y.-H. Lin, J. D. Surratt, P. Zotter, A. S. H. Prévôt, and R. J. Weber (2011), Light-absorbing soluble organic aerosol in Los Angeles and Atlanta: A contrast in secondary organic aerosol, *Geophys. Res. Lett.*, *38*, L21810, doi:10.1029/2011GL049385.
- Zhang, X. L., Y. H. Lin, J. D. Surratt, and R. J. Weber (2013), Sources, composition and absorption Angstrom exponent of light-absorbing organic components in aerosol extracts from the Los Angeles Basin, *Environ. Sci. Technol.*, *47*, 3685–3693.
- Zhang, Y., J. Li, G. Zhang, P. Zotter, R.-J. Huang, J.-H. Tang, L. Wacker, A. S. H. Prévôt, and S. Szidat (2014), Radiocarbon-based source apportionment of carbonaceous aerosols at a regional site on Hainan Island, South China, *Environ. Sci. Technol.*, *48*, 2651–2659.
- Zhong, M., and M. Jang (2014), Dynamic light absorption of biomass burning organic carbon photochemically aged under natural sunlight, *Atmos. Chem. Phys.*, *14*, 1517–1525.